

ANALYSIS OF THE H_2^+ WITH H_2 REACTION
USING ELECTRON NUCLEAR DYNAMICS

By
JUAN OREIRO

A DISSERTATION PRESENTED TO THE GRADUATE SCHOOL
OF THE UNIVERSITY OF FLORIDA IN PARTIAL FULFILLMENT
OF THE REQUIREMENTS FOR THE DEGREE OF
DOCTOR OF PHILOSOPHY

UNIVERSITY OF FLORIDA

1997

In memory of Maria Augusta.

ACKNOWLEDGMENTS

I would like to thank my advisor, Professor Yngve Öhrn, for his always encouraging, warm, and inspiring attitude, not only in science but also in a personal level. I also wish to acknowledge the support, enthusiasm, and guidance of Dr. Erik Deumens who is always in a good mood despite my repeated attempts to bring chaos onto his neat computer network.

Of course, this work would not be possible without the help and the many discussions with the rest of the Öhrn-Deumens group. I thank, in particular, Augie Diz, Ricardo Longo, and Hugh Taylor for their invaluable help and exchange of ideas. I couldn't forget to mention Monique Chacon-Taylor, who made things make more sense with her "Margarita nights," albeit I couldn't remember much in the morning.

Finally, I would like to extend my gratitude to the other QTP members and personnel for creating a both stimulating and fun environment to do research.

TABLE OF CONTENTS

	page
ACKNOWLEDGMENTS	iii
LIST OF TABLES	vi
LIST OF FIGURES	viii
ABSTRACT	xiii
1 INTRODUCTION	1
2 THEORETICAL, TIME-DEPENDENT APPROACHES TO MOLECULAR DYNAMICS	11
Classical Approach.....	11
Semiclassical Approaches.....	13
Quantum Mechanical Approaches.....	15
3 THE ELECTRON-NUCLEAR DYNAMICS (END) FORMALISM	17
Method.....	17
Electronic and Nuclear Descriptions.....	18
The END Equations of Motion.....	19
4 BIBLIOGRAPHIC REVIEW	25
Collision Induced Dissociation.....	25
Charge Transfer.....	28
5 BASIS SETS AND ENERGETICS	31
Basis and H_4^+	31
STO-3G Basis	35
Dunning's DZ Basis	36
Dunning's pVDZ Basis	36
Energetics.....	37
6 CROSS-SECTIONS	44
The Collinear Approximation.....	45

Collision Induced Dissociation	48
Charge Transfer	52
Full Reaction Space	58
Collision Induced Dissociation	59
Charge Transfer	65
Comparison with Molecular Dynamics	70
Final Probabilities	71
pVDZ basis	76
7 CONCLUSIONS	79
LIST OF REFERENCES	82
BIOGRAPHICAL SKETCH	90

LIST OF TABLES

Table	page
Table 5-1: Contraction coefficients (c) and exponents (α) for the STO-3G basis.	36
Table 5-2: Contraction coefficients (c) and exponents (α) for Dunnin's pVDZ basis, with scaling factor 1.44.	36
Table 5-3: Total energies, in atomic units, for the ground states.	37
Table 5-4: Bond lengths for the equilibrium geometries in the STO-3G basis, values in atomic units.	38
Table 5-5: Bond lengths for the equilibrium geometries in the DZ basis, values in atomic units.	38
Table 5-6: Bond lengths for the equilibrium geometries in the pVDZ basis, values in atomic units.	38
Table 5-7: Energetics in kcal/mol. Energy required to break H_4^+ into $H_2^+ + H_2$, $H_3^+ + H$, and total energy released by CID, respectively.	39
Table 6-1: CID cros-sections, in \AA^2 , for 0.519 eV (CM), DZ basis.	51
Table 6-2: CT cros-sections, in \AA^2 , for 0.519 eV (CM), DZ basis.	58
Table 6-3: CID cros-sections, in \AA^2 , for 4 eV (CM), STO-3G basis.	64

Table 6-4: CT cross-sections, in \AA^2 , for 4 eV (CM), STO-3G basis	70
Table 6-5: Probabilities for the final electronic configurations with initial conditions 606060 (4 eV, STO- 3G). The shaded box displays the highest mixed character and a comparison between END and dynamics on a surface is provided for this case. (a, b are the impact parameters; CT: charge transfer; NR: non-reactive)	72

LIST OF FIGURES

Figure	page
Figure 5-1: Available channels and cross-sections (\AA^2) for energies 0.1 to 10^5 eV (lab)	33
Figure 5-2: Cross-sections (\AA^2) for the range of energies studied, 1-8 eV (lab)	34
Figure 5-3: Energetics for the STO-3G, DZ, and pVDZ bases sets.	40
Figure 5-4: UHF ground-state surfaces for the STO-3G, DZ, and pVDZ bases	41
Figure 5-5: Bond lengths diagram for the H_3^+ and H_4^+ species in the D_{3h} and C_{2v} geometries, respectively.....	42
Figure 6-1: Degrees of freedom for the $\text{H}_2^+ + \text{H}_2$ reaction: α and β are the projectile and target tilt angles, respectively; γ is the dihedral angle; a and b are the impact parameters in the x and y directions, respectively.	45
Figure 6-2: Collinear series, 0.519 eV, DZ basis, impact parameter 5 a. u.; top panel: nuclei trajectories on the xy plane; center panel: bond lengths vs. time; bottom panel: total Mulliken populations vs. time (all data in a. u.)	49
Figure 6-3: Collinear series, 0.519 eV, DZ basis, impact parameter 3 a. u.; top panel: nuclei trajectories on the xy plane; center panel: bond lengths vs. time; bottom	

panel: total Mulliken populations vs. time (all data in a. u.)	50
Figure 6-4: Collinear series, 0.519 eV, DZ basis, impact parameter 0.5 a. u.; top panel: nuclei trajectories on the xy plane; center panel: bond lengths vs. time; bottom panel: total Mulliken populations vs. time (all data in a. u.)	53
Figure 6-5: Collinear series, 0.519 eV, DZ basis; the projectile (H_2^+) total Mulliken population, as a function of time and impact parameter (all data in a. u.)	55
Figure 6-6: Collinear series, 0.519 eV, DZ basis; the projectile (H_2^+) bond length, as a function of time and impact parameter (all data in a. u.)	56
Figure 6-7: Collinear series, 0.519 eV, DZ basis, impact parameter 0.3 a. u.; top panel: nuclei trajectories on the xy plane; center panel: bond lengths vs. time; bottom panel: total Mulliken populations vs. time (all data in a. u.)	57
Figure 6-8: Bond breaking profiles for collision energy 4 eV and STO-3G basis; the shaded area marks the probability for the CID channel, as a function of both impact parameters (in a. u.); each series is labeled as xxyyzz, where xx is the projectile tilt angle, yy the target tilt angle, and zz the dihedral angle, all in degrees.	60
Figure 6-9: Bond breaking profiles for collision energy 4 eV and STO-3G basis; the shaded area marks the probability for the CID channel, as a function of both impact	

parameters (in a. u.); each series is labeled as $xyyzz$, where xx is the projectile tilt angle, yy the target tilt angle, and zz the dihedral angle, all in degrees. 61

Figure 6-10: Bond breaking profiles for collision energy 4 eV and STO-3G basis; the shaded area marks the probability for the CID channel, as a function of both impact parameters (in a. u.); each series is labeled as $xyyzz$, where xx is the projectile tilt angle, yy the target tilt angle, and zz the dihedral angle, all in degrees. 62

Figure 6-11: Bond breaking profiles for collision energy 4 eV and STO-3G basis; the shaded area marks the probability for the CID channel, as a function of both impact parameters (in a. u.); each series is labeled as $xyyzzz$, where xx is the projectile tilt angle, yy the target tilt angle, and zzz the dihedral angle, all in degrees. 63

Figure 6-12: Charge transfer profiles for collision energy 4 eV and STO-3G basis; the shaded area marks the probability for the CT channel, as a function of both impact parameters (in a. u.); each series is labeled as $xyyzz$, where xx is the projectile tilt angle, yy the target tilt angle, and zz the dihedral angle, all in degrees. 66

Figure 6-13: Charge transfer profiles for collision energy 4 eV and STO-3G basis; the shaded area marks the probability for the CT channel, as a function of both impact parameters (in a. u.); each series is labeled as $xyyzz$, where xx is the projectile tilt angle, yy the target tilt angle, and zz the dihedral angle, all in degrees. 67

- Figure 6-14: Charge transfer profiles for collision energy 4 eV and STO-3G basis; the shaded area marks the probability for the CT channel, as a function of both impact parameters (in a. u.); each series is labeled as *xyyyzz*, where *xx* is the projectile tilt angle, *yy* the target tilt angle, and *zz* the dihedral angle, all in degrees. 68
- Figure 6-15: Charge transfer profiles for collision energy 4 eV and STO-3G basis; the shaded area marks the probability for the CT channel, as a function of both impact parameters (in a. u.); each series is labeled as *xyyyzzz*, where *xx* is the projectile tilt angle, *yy* the target tilt angle, and *zzz* the dihedral angle, all in degrees. 69
- Figure 6-16: 606060 END series, 4 eV, STO-3G basis, impact parameters 3 and 0 a. u. (*y* and *z* axes, repectively); top panel: nuclei trajectories of the coordinates; center panel: bond lengths vs. time; bottom panel: total Mulliken populations vs. time (all data in a. u.) 74
- Figure 6-17: 606060 DRC series, 4 eV, STO-3G basis, impact parameters 3 and 0 a. u. (*y* and *z* axes, repectively); top panel: nuclei trajectories of the coordinates; center panel: bond lengths vs. time; bottom panel: total Mulliken populations vs. time (all data in a. u.) 75
- Figure 6-18: 000000 END series, 4 eV, pVDZ basis, impact parameters 0 and 4 a. u. (*y* and *z* axes, repectively); top panel: nuclei trajectories of the coordinates; center panel: bond lengths vs. time; bottom panel: total Mulliken populations vs. time (all data in a. u.) 77

Figure 6-19: 000000 DRC series, 4 eV, pVDZ basis, impact
parameters 0 and 4 a. u. (y and z axes, repectively); top
panel: nuclei trajectories of the coordinates; center
panel: bond lengths vs. time; bottom panel: total Mulliken
populations vs. time (all data in a. u.) 78

Abstract of Dissertation Presented to the Graduate School
of the University of Florida in Partial Fulfillment of the
Requirements for the Degree of Doctor of Philosophy

ANALYSIS OF THE H_2^+ WITH H_2 REACTION
USING ELECTRON NUCLEAR DYNAMICS

By

Juan Oreiro

December, 1997

Chairman: N. Yngve Öhrn
Major Department: Chemistry

The END formalism addresses the solution of the time-dependent Schrödinger equation, treating both electrons and nuclei simultaneously. It differs from the other traditional fully quantum mechanical time-dependent methods in that it does not require a potential energy surface (PES) to carry the nuclear motion. The interaction between electronic and nuclear motion is, therefore, obtained in a transparent way, not relying on PES gradients to obtain the coupling between electrons and nuclei.

We analyze the $H_2^+ + H_2$ reaction at energies below 4 eV using different approximations and basis sets. Other than the choice of initial conditions, form of wave function, and basis set, no constraints are imposed on the system evolution. The nuclei are treated in the classical limit, and the electronic part is described by a single determinantal, unrestricted wave function. We obtain properties, such as

Mulliken populations, transition probabilities, and cross-sections, from the resulting trajectories. These results are compared with other current theoretical approaches, and with experimental values. The relevance of the electron-nuclear coupling is estimated by comparing the END trajectories with molecular dynamics calculations for selected initial conditions in different basis sets.

CHAPTER 1 INTRODUCTION

Hydrogen is the most abundant element in the universe. Whenever matter begins to aggregate, the first molecules to form are H_2 and carbon, nitrogen, and oxygen hydrides. From dense interstellar clouds to the atmosphere of the Jovian planets, these molecules play a central role, and ultimately determine, the chemistry of the system.

On Earth, most of the hydrogen has escaped from the atmosphere. Its reactions do not affect us in a direct way. That did not prevent an early interest in hydrogen chemistry from developing. In particular, the reaction $H_2^+ + H_2$ has attracted a crowd of experimental and theoretical researchers alike. This enthusiasm is justified. The reaction is rich in features, yet simple enough to allow an understanding of its driving principles. A great number of chemical processes is displayed by $H_2^+ + H_2$. Long-range Coulomb forces, selective vibrational enhancement, multi-channel competition at low energies, are among the many features present.

The ability to predict the outcome of a reaction, based on its initial conditions, constitutes the very core of chemistry. In this context, the meaning of "outcome" has undergone an update in the last few years with the advent of

feasible time-dependent methods on the theoretical side and femtosecond spectroscopic techniques in the lab.

Again, the $\text{H}_2^+ + \text{H}_2$ processes provide an excellent opportunity to put those new tools to the test. At collision energies of about 8 eV (lab frame) or less, only two competing channels are present. The first one, commonly referred to as collision induced dissociation (CID), yields $\text{H}_3^+ + \text{H}$ as the product. The other channel involves an electron transfer from H_2 to H_2^+ , and is usually called the charge transfer (CT) reaction.

Above 8 eV, a multitude of channels is accessible but either CT or CID dominate in the range from 0 to 10^4 eV. Minor competition is offered by proton and electron production starting at around 8 and 100 eV, respectively, and the atomic Hydrogen Lyman and Balmer series at even higher energies. No experimental or theoretical data is available for energies above 10^4 eV and results in the lower end are scarce.

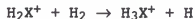
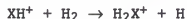
Each of the species involved in this reaction, either as a reactant, product, or intermediate, has a history of its own. The H_2 weak quadrupole transitions, initially measured by Herzberg in the infrared range[1], have become an important tool in identifying astronomical objects[2]. The hydrogen molecule has been widely studied by both theoretical and experimental methods. Its ground state vibrational and rotational spectra were analyzed in detail[3] and data is

available for even highly excited Rydberg states[4]. The H_2^+ ion is equally well known, being a common example in most introductory Quantum Chemistry texts.

J. J. Thomson was the first to observe the existence of H_3^+ in 1912 using a mass spectrometer coupled to his "positive rays" experiment[5]. Its preponderance over H_2^+ was soon explained by the highly efficient and exothermic CID reaction, which converts the latter to the triatomic ion[6]. Since its discovery, H_3^+ has puzzled chemists. For many years its structure was totally unknown, leading Eyring to refer to the problem as the "scandal of modern Chemistry[7]". Bohr was the first to publish a theoretical paper about the ion[8]. In the mid and late 30's Eyring, Hirschfelder[9], and collaborators suggested that H_3^+ exists in a triangular structure. However, it was not until 1973 that an accurate value for its ground state energy was made available[10]. It took a few more years and the, then new, technique of Coulomb explosion to establish its ground state as belonging to a C_{2v} point group[11]. A benchmark calculation employing an extensive Gaussian basis and a Hylleraas-type CI wave function was able to improve on these results by a few tenths of milihartree[12].

In recent years, the interest in H_3^+ has been revived. This triatomic has been found to be the main protonator agent in, and ultimately responsible for, all known interstellar chemistry[13]. A cascade of reactions in a highly ionizing

environment, where free electrons abound, form most of the common hydrides:



where X could be, for instance, O or C, and e^- is a free electron. It was also suggested that the abundance of H_3^+ could provide a measure of cosmic ray flux in an interstellar medium[14]. Due to its high rate of formation in hydrogen plasmas[15], its suppression is desirable in nuclear fusion[16].

It is surprising that for a molecule considered the simplest polyatomic and with only one barely stable electronic excited state[17], its spectrum was completely unknown until recently. Only in 1980 the first 15 spectral lines belonging to the ν_2 fundamental band were identified[18].

There is a wide selection of high-quality PES's available for the H_3 system, starting with the one obtained by Carney and Porter in 1974[19] and subsequently used to calculate the vibrational modes of H_3^+ [20]. Their work has been further improved and it is now possible to find even full CI surfaces, such as the Meyer-Botschwina-Burton (MBB) obtained with a (10s,4p,2d) Gaussian basis[21]. Very accurate fittings have been obtained for those PES's. There are no detectable discrepancies between experimental and theoretical

spectroscopic results based on those analytical expansions. In fact, these calculations have been used to predict ro-vibrational lines beyond the limits of the available experimental apparatus[22, 23]. These highly accurate potentials have made H_3^+ a favorite target for studies.

Another participating species, H_4^+ , has been no less controversial. Deemed as non-stable for many years, it was only observed experimentally in 1984[24], after detailed *ab initio* calculations suggested the structure was viable[25-27]. Now, it is known that H_4^+ is not only stable, but its ground state PES is capable of holding several vibrational levels. Its lifetime is of the order of microseconds.

A favorite topic of discussion seems to be whether H_4^+ can be obtained from the $H_2 + H_2^+$ reaction. According to current consensus, it can only be generated from breaking heavier clusters. This is based on experimental observations and no reasonable theoretical explanation seems to exist that can support this belief. If H_4^+ were to be formed, due to its shallow ground state minimum, it would likely be found at low collision energies. No reliable calculations have been performed for collisions energies below 2 eV (lab frame). The difficulties associated with measuring a low-stability charged species might account for its absence in the list of products. This ion exists in a supermolecule-like ground state. The H_3^+ ion, in an almost C_{2v} geometry, is orbited by a H atom which lies far away aligned to one of the triangle

vertices. Conventional detection techniques, such as those used in time of flight (TOF) measurements, would allow smaller charged ions to interfere, a problem known to exist for H_2^+ and H_3^+ . That would be less likely to occur when H_4^+ is the result of splitting a heavier cluster, and might explain why it has been detected that way. The possibility of breakage into $H_3^+ + H$ should not be discarded either, due to the relatively long times required for some detection methods.

Unlike the situation for H_3^+ , there are not that many potential energy surfaces available for the H_4^+ system. The higher number of geometrical conformations to be spanned makes the work of mapping the reaction space both tedious and costly. Accurate fitting is also significantly more complex. The situation is even worse for excited electronic states, required to describe electron transfer properly. That fact might explain the dominant position of the CID channel as compared to CT, which has been borne out in a number of published studies. The inclusion of even simple excited states, such as the ones obtained via self-consistent field (SCF) or singles and doubles configuration interaction (SD-CI,) seems to provide good results. It allows for the correct behavior in the CT channel, i.e., an increase of the cross section with the impact energy, and a decrease with the impact parameter[28].

Although models developed within stationary-state frameworks have dominated Theoretical Chemistry in the past, frequently yielding excellent results, a full understanding of a chemical reaction encompasses its evolution in time. A dynamical process, with spectroscopic and structural properties evolving continuously, needs a time-dependent treatment. As successful as traditional approaches to molecular dynamics have been, these did not possess the tools to allow an insight into the reaction mechanisms in terms of basic principles. They have frequently resorted to extraneous assumptions in order to achieve a simple theoretical structure.

The inception of time-dependent methods is not recent, but until the last decade they could not be classified as working tools. Both computational and theoretical problems contributed to this delay.

For similar reasons, Chemistry has been depicted in terms of mostly adiabatic processes. Both the convenience and the success of the Born-Oppenheimer approximation have led to the belief that the coupling between electronic and nuclear motion was either small enough to be negligible or confined to short segments of a reaction. As a consequence, the Potential Energy Surface picture flourished and it is almost impossible not to rely on it when discussing chemical processes. That well established view has been challenged more intensely in the last few years. A particular example being the study of charge transfer. The refinement of

existing experimental techniques and the introduction of new ones made more apparent the deficiency of older models. The increased computer power allowed the development of new ones.

The Electron-Nuclear Dynamics (END)[29] theoretical framework, goes beyond the above restrictions. It allows for a full and instantaneous interaction between electrons and nuclei, while developing approximations to the time-dependent Schrödinger equation. The END equations have been coded into the software package ENDyne and will be discussed in some detail later. The analysis of the resulting evolution is done by the program Evolve, which was revised for this study.

In its present incarnation, END employs a single determinant built from spin-unrestricted orbitals with complex coefficients to describe the electrons. The nuclei are considered in the limit of narrow wave-packets. The system evolution proceeds without the need for a PES. Not only does that save computer time but also eliminates inaccuracies due to the fitting procedure. It is a one-step, general process. Traditional methods involve three steps: calculation of the PES, fitting of the surface, and carrying out the dynamics. (The second of them frequently is property or application oriented.) With END it is possible to calculate systems for which no PES exist and retrieve most properties, as a function of time, from the resulting wave function.

Despite being investigated by an unusually high number of experimental techniques and theoretical approaches, the

reaction of H_2^+ with H_2 is still a challenge. The fact that the system is the simplest one involving a charged and a neutral molecule could not explain alone the intense interest it has motivated. The existence of a high quality PES, and analytical fittings for those, has certainly helped to attract part of the crowd of dynamicists eager to test their approaches in a reaction with more than three nuclei. Reliable PES for systems with four or more atoms are still an exception at this time. Since most of the available approaches for molecular dynamics rely on one or more PES's, systems for which such surfaces exist are always a preferred target. The vast number of experimental results available for this reaction has also contributed to intensify the efforts of studying it using a variety of theoretical techniques.

A fully quantum-mechanical, three-dimensional study was published only recently on the subject[30]. The authors calculated both the reactive and the charge transfer cross sections for two values of collisional energy (0.252 eV and 0.519 eV). They used only 14 randomly selected initial geometries due to the high computational demand of the problem. Their results agree remarkably well with experimental measurements for the reactive cross section, but not for the charge transfer (CT) one. Several reasons come to mind to explain the failure in predicting the CT cross section. It might be an intrinsic limitation of their approach (Infinite Order Sudden Approximation - IOSA), an inaccuracy due to the rather limited sampling of the reaction

space, a basis set artifact, a feature of the potential energy surface or fitting employed, or a combination of any of those and other factors.

Also, even for the reactive cross section, there are many details that are not clear or could be explored more deeply. In order to do that, we decided to carry out calculations on the H_2^+ with H_2 reaction using the END approach.

CHAPTER 2 THEORETICAL, TIME-DEPENDENT APPROACHES TO MOLECULAR DYNAMICS

Classical Approach

The classical approach to molecular dynamics consists of two steps: the determination of the potential energy surface (PES) and the numerical tracing of the collision trajectories on that surface, following classical equations of motion. The latter is a rather trivial procedure, especially with the fast computers available now. The generation of the PES and its fitting is the crucial part of this method. Despite the fact that only one PES is required, the accurate representation of the potential topology is still a demanding task for most systems containing more than three atoms. In addition, processes involving multiple PES's are not adequately treated within this framework. There is a great number of processes that are not adiabatic, among them, charge-transfer, electronic energy transfer, collisional quenching, spin-forbidden reactions, and radiationless transitions. To accurately depict such phenomena one has to include not only all the PES's involved, but also the couplings between those surfaces[31]. Also, processes where quantum effects are noticeable cannot be correctly described,

those include systems for which tunneling and zero-point energy are important.

The usual way to obtain the potential is through *ab initio* calculations, although semiempirical and even empirical methods have also been employed[32]. The discrete set of energies must then be converted to a more suitable analytical form, in order to allow for the rapid evaluation of the derivatives of the potential energy. However, the large number of nuclear configurations involved in a molecular collision precludes the calculation of a complete surface, even for systems for which accurate energies can be obtained. The fitting must be based on a limited set of geometries, usually chosen by convenience or symmetry considerations. According to McLaughlin and Thompson[33]:

"...The calculation of surfaces remains somewhat of a stumbling block to a completely *ab initio* approach to classical dynamical studies of chemical dynamics."

The fitting of PES's has become a favorite topic of interest by itself and some examples can be found in the study on 2D cubic spline interpolation by Sathyamurthy, Kellerhals, and Raff[34], the scattering calculations for $\text{He} + \text{H}_2^+$ by Sathyamurthy, Rangarajan, and Raff[35], or the $\text{H} + \text{H}_2$ reaction using classical trajectories by Gray and Wright[36].

Semiclassical Approaches

This class of approaches comprises methods that employ simple approximate procedures to extend the validity of the classical models. They provide a better description of the molecular dynamics in the sense that one is no longer limited to purely adiabatic effects. In their most common implementation, two PES's are used. The coupling between the two surfaces is normally introduced in an *ad hoc* way. The evolution is carried out until a certain point of the trajectory is reached, where diabatic effects are believed important. At that point, a somewhat arbitrary procedure is used to trigger the surface hopping. How well the technique describes the system depends on how accurately the transition point is chosen and how good the guess for the coupling between the PES's is. The same limitations concerning the calculation and fitting of the potential surfaces apply, with the extra complication that now more than one surface is needed and they will not be necessarily of the same quality.

One popular implementation of the semiclassical methodology is due to Miller and George[37] and it's aimed at describing electronic transitions in low energy atomic and molecular collisions, or involving quantized degrees of freedom. Their framework is based on the integration of Hamilton's equations using complex-valued time. Both coordinates and momenta are allowed to take on complex values and the transition happens when a trajectory crosses a branch

point (corresponding to an adiabatic surface intersection). The approach relies on the Feynman propagator and involves the construction of complex-valued time contours to find a hopping point. It is assumed that at low energy the dynamics is essentially a classical single-surface phenomena, with transitions being isolated events that happen in localized points of space and time.

Another common technique was devised by Tully and Preston[38] and called the "surface hopping" method. It differs from the Miller and George approach in that the momentum is not required to be a smooth function of time. Rather, the momentum changes abruptly when an avoided crossing is reached, to allow for the propagation on the different PES. The main advantage in this case is that one does not have to deal with the complex-valued trajectories.

Both techniques have been shown to be equivalent, provided there are only two surfaces involved in the crossing, the splitting of the surfaces may be expressed as a function of a single variable, and the trajectories have no turning points close to the intersection ("high energy limit") [39].

There's a great number of papers applying semiclassical methods, particularly surface hopping and its variations, to light systems. The semiclassical approach is sometimes called quasiclassical in these studies[40-45].

Quantum Mechanical Approaches

This class of methods, unlike the previous ones, rely on fully quantum mechanical equations of motion. Coupling between different surfaces arise naturally and do not depend on predefined transition schemes.

Presently, there are two main approaches in the literature for quantum mechanical evolutions on potential surfaces. The first one was proposed by M. Baer and co-workers and it is referred to simply as the quantum mechanical (QM) method. It's based on what the authors call "the negative imaginary decoupling potentials" (NIPD) to convert multi-arrangement channels into inelastic single-arrangement systems, in order to reduce the configuration space. The inelastic collision is then treated by means of the infinite order sudden approximation (IOSA).

That method has been applied to a number of collinear and three-dimensional systems[46, 47]. Baer and Ng[30] have published the only paper where the full dimensionality of the $\text{H}_2^+ + \text{H}_2$ reaction was taken into account in a quantum mechanical level, where they have used 28 randomly selected configurations (initial relative molecular orientations).

The second approach in use is usually referred to as exact quantum mechanical methods[48, 49]. They are "exact" in the sense that the error could, in principle, be made as small as required. This is in practice frustrated by computational constraints. In order to represent the system

wave function, a basis of a numerical grid and weights is required. The smaller the interval between the grid points, the better the accuracy achieved. The total size of the grid is also important, since boundary effects may compromise the results. It is frequently not possible to generate the grid with dimensions large enough to describe the reaction going on. Wave packets can approach the rim of the grid and impart non physical effects to the dynamics. To minimize that, one has to apply "cushion" potentials to simulate a natural exit for the reactants. Exact methods give excellent results when they can be applied. Currently, the larger systems studied with this technique consist of six atoms.

CHAPTER 3 THE ELECTRON-NUCLEAR DYNAMICS (END) FORMALISM

Method

The END formalism addresses the solution of the time-dependent Schrödinger equation, treating both electrons and nuclei simultaneously. It differs from other traditional fully quantum mechanical time-dependent methods in that it does not require a PES to carry the nuclear motion. The interaction between electronic and nuclear motion is therefore obtained in a transparent way, not relying on PES gradients to obtain the coupling between electrons and nuclei.

There are several advantages in not depending on PES. First, there is no need to calculate such surfaces *per se*. For mid-sized and large systems, obtaining a good PES is a major task. With several degrees of freedom, it can easily be the most time-consuming part of the calculation. Commonly, the groups who work on dynamics are not the ones who generate the PES. That creates two problems. First, the dynamicists don't have control over the PES quality. Second, they are limited to whatever data is available. The actual calculation of the surface is just one of the steps, however. The data is given in a set of points that must be interpolated and

extrapolated to provide the necessary surface. The quality of the interpolation is critical to obtain a good representation of the dynamical event. So, another source of errors is introduced, over which one has little control. Besides, a chemical process frequently requires the use of several surfaces, corresponding to different electronic states. That is especially true at higher energies. Finding one high-quality PES is difficult, finding several of them for the same system is almost a unique event.

END is based on the Time-Dependent Variational principle (TDVP)[50], with a wave function parametrized in terms of Coherent States[51, 52]. The main advantage of using Coherent States is that one gets simplified equations, non-redundant parameters in the definition of the electronic state, and it is easier to interpret the results. This kind of parametrization also guarantees that all wavefunctions of a particular family can be reached, should the dynamics so require.

The END formalism has been implemented in the program ENDDyne[29] for a number of wave functions, with some restrictions and approximations which will be discussed below.

Electronic and Nuclear Descriptions

As it is now, ENDDyne is limited to treat nuclei as classical particles. This corresponds to the limit of infinitely narrow gaussian wave packets and defines their

time-dependent variables as their positions and momenta and retains all nonadiabatic coupling terms. The electronic part is expressed in terms of a truncated Gaussian basis and is restricted to single-determinantal wave functions. The formalism for a multi-determinantal electronic description is developed and under implementation[53].

That means that we can set the initial conditions for an evolution as a set of generalized coordinates for the nuclei and an electronic state, the latter expressed in terms of complex spin-orbital coefficients. The only additional data needed are the mass of the nuclei and their atomic number.

There are three different choices for the electronic wave function presently available: a restricted single-determinantal wavefunction, with either pure-spin orbitals or mixed-spin orbitals. A two-level model, for both classical quantum (Gaussian) nuclei is available. In this work we use the unrestricted description with the pure-spin option.

The END Equations of Motion

Here we don't give a detailed derivation of the END equations but just show the structure of them and where they come from. We are going to outline the expressions built in the ENDyne code. Instead of considering the most general case, we will limit ourselves to classical nuclei and assume that the electronic part of the wave function can be described by a complex, spin-unrestricted determinant. A

rigorous and more general account of the formalism behind the method can be found in the references listed previously.

In our case, the atomic spin orbitals (AOs) are given by a set of Gaussians,

$$u_i(\vec{r}) = x^k y^l z^m \exp\left[-b(\vec{r} - \vec{r}_0)^2\right] \quad (3.1)$$

with an appropriate spin part, α or β , attached to them. We can define a general, complex spin orbital for the electrons as

$$\psi(\vec{r}) = \sum_{i=1}^K u_i(\vec{r}) c_i, \quad (3.2)$$

where the total number of AOs, K , consists half of α and half of β orbitals.

For a Coherent State wave function $|\zeta\rangle$, defined by a set of parameters $\{\zeta\}$, we can write the first variation of the quantum mechanical action functional, A , as

$$\delta A = \delta \int \left\{ \frac{i\hbar}{2} \left[\langle \zeta | \frac{d}{dt} |\zeta \rangle - \frac{d}{dt} (\langle \zeta |) \langle \zeta \rangle \right] - \langle \zeta | H | \zeta \rangle \right\} \langle \zeta | \zeta \rangle^{-1} dt \quad (3.3)$$

and the solutions we look for are the ones for which $\delta A = 0$, according to the TDVP (principle of least action).

By introducing the functions $E(\zeta, \zeta^*) = \langle \zeta | H | \zeta \rangle / \langle \zeta | \zeta \rangle$ and

$S(\zeta, \zeta^*) = \langle \zeta | \zeta \rangle$ for the total energy and overlap, respectively,

and setting $\hbar=1$, after several algebraic steps we can rewrite the first variation of the action functional as

$$\delta A = \int \left[\sum_{\beta} \left\{ \sum_{\alpha} \left(-i \frac{\partial^2 \ln S}{\partial \zeta_{\alpha}^* \partial \zeta_{\beta}} \zeta_{\alpha}^* - \frac{\partial E}{\partial \zeta_{\beta}^*} \right) \delta \zeta_{\beta}^* + \sum_{\alpha} \left(i \frac{\partial^2 \ln S}{\partial \zeta_{\alpha} \partial \zeta_{\beta}^*} \right) \delta \zeta_{\beta}^* \right\} \right] dt = 0, \quad (3.4)$$

where the $\dot{\zeta}$ denotes differentiation of the complex parameter with respect to time.

The solution of the TDVP expression will then be the dynamical equations given by

$$\begin{pmatrix} iC & 0 \\ 0 & -iC^* \end{pmatrix} \begin{pmatrix} \dot{\zeta} \\ \dot{\zeta}^* \end{pmatrix} = \begin{pmatrix} \partial E / \partial \zeta^* \\ \partial E / \partial \zeta \end{pmatrix}, \quad (3.5)$$

where we define the general element of the hermitian matrix C as $C_{\alpha\beta} = \partial^2 \ln S / \partial \zeta_\alpha \partial \zeta_\beta^*$.

There are a few ways one can choose the electronic basis dependence on the nuclear motion. Three of the most useful choices are called the nonfollowing basis (NFB), the static following basis (SFB), and the dynamic following basis (DFB). In the limit of a complete basis set, the three types are equivalent. However, actual calculations are carried out in truncated basis sets, with a finite number of orbitals. The three bases will not necessarily yield the same results under those circumstances.

A NFB is one for which the basis grid is fixed in time and space, the electronic orbitals do not move at all during the system evolution. The equations of motion assume their simplest form in this case. This is the ideal choice for carrying the algebraic manipulations and interpreting the equations, if one can assume completeness.

A SFB is one for which the basis are centered on the average position of the nuclear wave packets, or the nuclear coordinates in the limit of infinitely narrow wave packets.

The AOs do not carry an explicit term containing the orbital velocity in these cases, they just follow the nuclei.

A DFB is one for which the AOs are defined in such a way that they have an intrinsic velocity and their positions change with time. The velocities are embodied in factors with the properties of a plane wave and are usually referred to as electron translation factors (ETFs)[54]. Those terms are known to play an important rôle in high energy collisions. The general form of an AO (omitting spin), including the ETF would be

$$u_i(\vec{r}) = x^k y^l z^m \exp \left[-b(\vec{r} - \vec{r}_0)^2 + im_e \vec{v}_0 \cdot \vec{r} \right]. \quad (3.6)$$

Saying that the three bases above are equivalent in the completeness limit amounts to stating that their equations yield the same dynamics. Their metrics are the same. They can be therefore related by a transformation that does not change the metric. Such transformation is referred to as a symplectic one (or canonical, when the metric only contains zeroes and ones).

At this point, ENDyne does not include ETFs in its equations, but a SFB representation is used. Ordinary chemistry takes place at relatively low energies. We therefore don't expect ETFs contributing significantly to the study proposed here. The omission of such factors have a negligible effect in the final results. (Their effect is

taken into account approximately by the basis chosen, since the MO coefficients are complex.)

For NFB, the equations of motion with real nuclear coordinates, \mathbf{R} , and momenta, \mathbf{P} , become (\mathbf{z} are the Thouless parameters for the electrons), [55]

$$\begin{pmatrix} iC & 0 & 0 & 0 \\ 0 & -iC^* & 0 & 0 \\ 0 & 0 & 0 & -I \\ 0 & 0 & I & 0 \end{pmatrix} \begin{pmatrix} \dot{\mathbf{z}} \\ \dot{\mathbf{z}}^* \\ \dot{\mathbf{R}} \\ \dot{\mathbf{P}} \end{pmatrix} = \begin{pmatrix} \partial E / \partial \mathbf{z}^* \\ \partial E / \partial \mathbf{z} \\ \partial E / \partial \mathbf{R} \\ \partial E / \partial \mathbf{P} \end{pmatrix} \quad (3.7)$$

yielding the individual equations,

$$C\dot{\mathbf{z}} = -i \frac{\partial E}{\partial \mathbf{z}^*}, \quad (3.8)$$

$$\dot{\mathbf{P}}_k = -\nabla_{\mathbf{R}_k} E, \text{ and} \quad (3.9)$$

$$\dot{\mathbf{R}}_k = \frac{\mathbf{P}_k}{M_k}. \quad (3.10)$$

Assuming a complete basis, we can obtain the equivalent result for a SFB, after a symplectic transformation, as

$$\begin{pmatrix} iC & 0 & iC_R & 0 \\ 0 & -C^* & -iC_R^* & 0 \\ iC_R^* & -iC_R^T & C_{RR} & -I \\ 0 & 0 & I & 0 \end{pmatrix} \begin{pmatrix} \dot{\tilde{\mathbf{z}}} \\ \dot{\tilde{\mathbf{z}}}^* \\ \dot{\tilde{\mathbf{R}}} \\ \dot{\tilde{\mathbf{P}}} \end{pmatrix} = \begin{pmatrix} \partial E / \partial \tilde{\mathbf{z}}^* \\ \partial E / \partial \tilde{\mathbf{z}} \\ \partial E / \partial \tilde{\mathbf{R}} \\ \partial E / \partial \tilde{\mathbf{P}} \end{pmatrix}, \quad (3.11)$$

where \mathbf{I} is the identity matrix, $\tilde{\mathbf{z}}$ denotes a Thouless parameter in the SFB and the following definitions were made,

$$C_{X_k} \equiv \frac{\partial^2 \ln S(\tilde{\mathbf{z}}^*, R, P, \tilde{\mathbf{z}}, R', P')}{\partial \tilde{\mathbf{z}} \partial X_k} \bigg|_{R'=R, P'=P}, \quad (3.12)$$

and

$$C_{X,Y_l} \equiv -2\text{Im} \frac{\partial^2 \ln S(\tilde{z}, R, P, \tilde{z}', R', P')}{\partial X_k \partial Y_l'} \bigg|_{R'=R, P'=P} . \quad (3.13)$$

The individual equations in vector form for this case are therefore,

$$C\dot{z} + C_{R_l} \dot{\mathbf{R}}_l = -i \frac{\partial E}{\partial \tilde{z}} \quad (3.14)$$

$$\dot{\mathbf{P}}_k + 2\text{Im} C_{R_k}^* \dot{\tilde{z}} - C_{R_l R_l} \dot{\mathbf{R}}_l = -\nabla_{R_l} E \quad (3.15)$$

$$\dot{\mathbf{R}}_k = \frac{\mathbf{P}_k}{M_k} \quad (3.16)$$

Those are the equations coded in the ENDyne program package, where a summation over the nuclear coordinates label, l , is implied. C_R and C_{RR} are simply the so called nonadiabatic correction terms, that in the END theory appear in the dynamical metric.

CHAPTER 4 BIBLIOGRAPHIC REVIEW

Collision Induced Dissociation

The reaction $\text{H}_2^+ + \text{H}_2 \rightarrow \text{H}_3^+ + \text{H}$ has been extensively studied over the years. Its importance in interstellar[56] and atmospheric chemistry[57], as well as its suitability for rigorous theoretical treatment, account for part of the interest. Collision induced dissociation (CID) between ion and molecules are part of a class of reactions generally referred to as collisional energy transfer. However, they differ from the most general case in two important aspects: first, the amount of energy transferred is large enough to comprise a significant part of the translational energy; second, the reaction mechanism may be complex, involving several electronic surfaces and competing reaction channels[58].

Experimentally the H_3^+ system has been studied by crossed beam[59, 60], mass spectrometric[61, 62], merged beam[63, 64], photoionization[65], ICR[66], and ion beam-gas cell[67] techniques. These experiments showed the reaction to be exoergic by 1.7 eV and, contrary to initial beliefs, proceeding through a direct mechanism[63, 59, 60] where no barrier is involved[63, 64] and confirming the instability of

H_4^+ with respect to the $H_3^+ + H$ products[68]. In addition, its total cross-section was found to be very large at thermal energies, and to fall off rapidly with increasing collision energy[63, 64].

In principle, there would be two ways for the collision induced dissociation to proceed. The H_3^+ product could be formed by either proton or by a H atom transfer. The first mechanism would involve the breakage of the H_2^+ ion (requiring approximately 2.6 eV,) while the second would entail the rupture of the H_2 molecule (4.5 eV.) Energetics alone would make it seem more likely to have a predominance of the proton transfer. Trajectory surface hopping calculations have shown this to be true[69], the H_2^+ rupture not only dominates but it seems to be the exclusive mechanism for the reaction. Attempts to confirm this experimentally, by using isotopic substitution, have yielded a very different picture. It was found that both mechanisms occur, and have comparable cross-sections, apparently due to intensive charge transfer between the reagents[63, 69, 60, 59].

Photoionization experiments have shown that at collision energies below 1 eV (center of mass,) the H_3^+ formation can be inhibited by vibrationally exciting the H_2^+ ion[70, 65]. At higher energies, the opposite seems to hold. The reason for this behavior has been explained in terms of the interaction of several potential energy surfaces[60, 59, 71], putting a rigorous treatment of the problem out of reach of most current theoretical methods. Such interaction appears to be

the underlying cause for the competing mechanisms found in experiments involving isotopic substitution. The $(\text{H}_2 + \text{D}_2)^+$ ground PES could be entered by two alternative paths, one belonging to $\text{H}_2^+ + \text{D}_2$, the other to $\text{D}_2^+ + \text{H}_2$. At infinite separation each channel would have its own PES, but as they approach, making the ion and the neutral bond equal, an avoided crossing puts them on the same ground PES. The barrier between the two PES decreases until it becomes smaller than the reagent zero-point energy, which happens at 8-10 Bohr. At this point charge hopping between the two channels sets in [72, 59, 60, 27], accounting for the formation of both D_2H^+ and H_2D^+ .

The multiple surface nature of the H_4^+ system also further complicates the comparison between experimental and theoretical results. Most experiments involving electron bombardment are likely to excite the H_2^+ ion, populating higher vibrational states. Such experiments include crossed and merged beam studies [63, 64], and their results should be considered as involving all the accessible potential energy surfaces [73].

The CID channel was also explored with the molecular beam technique, using the enhanced four-photon ionization to prepare the H_2^+ ion in selected vibrational state distributions, for collision energies ranging from 1.5 to 5.3 eV (c.m.) [74]. The resulting data included the state-selected integral and differential cross sections. On a different experiment, using the merging beams technique, Lees and

Rol[64], obtained the reaction cross sections for several isotopic substitutions, at energies below 10 eV.

Charge Transfer

When a charge transfer (CT) process involving an ion and a molecule is exothermic, it is usually the dominant product channel for the reaction. Due to the large CT cross-sections, these reactions play a major role in both relaxation processes and reaction kinetics in ionized gases. The understanding of this class of processes is of special interest to gas discharges, lasers, flames, and controlled thermonuclear fusion. Although present in low concentration in flames, the ions are responsible for the thermal charge exchange reactions which create free radical chain carriers.

For collisions between molecular ions and molecules, where spatial orientation provides an extra challenge in generating the interaction potentials, the availability of reliable potential energy surfaces has been one of the major stumbling blocks for theoretical treatments aiming at obtaining accurate cross-sections. For the H_4^+ system, a number of PES has been made available, mostly for the ground state[75, 27, 71, 72, 28, 25].

On the experimental side, the challenges have not been smaller. Most of the studies done involve the measurement of cross sections as a function of the kinetic energy, and preparing the H_2^+ ion by electron ionization[76, 77, 61, 78-86]. The H_2^+ ions formed by electron ionization usually have a

broad distribution of vibrational states. Experimental results seem to indicate that a strong dependence of the cross section on the vibrational population of H_2^+ is to be expected[76, 77]. This finding, with the difficulty in obtaining reliable PES, has hindered the efforts to obtain a sound comparison between experiment and theory. For that reason, in recent years, the preferred empirical approach to prepare the system in well characterized distribution of states has become photoionization[87].

It is worth pointing out that most of the available reliable experimental results concentrate on higher collision energies, in particular above 200 eV[88]. One explanation might be the suggested poor resolution of the time-of-flight (TOF) analysis at low energies. Due to inelastic charge transfer channels, the slow H_2^+ products can be scattered by more than 10° away from the initial neutral H_2 beam direction[89]. The collection efficiency in the TOF analysis for product ions scattered at wide angles is poor. In addition, inelastic charge transfer can also lead the arrival of the H_2^+ product ions to be spread in time. As a result, for the reaction $H_2^+ + H_2$, the TOF does not provide a reliable detection method at energies below 8 eV (center of mass), since it cannot distinguish between the H_3^+ and the H_2^+ ions.

To circumvent those problems, Liao, Liao, and Ng[87], develop a ion-molecule reaction apparatus which combined the crossed ion-neutral beam method, high resolution photoionization mass spectroscopy, and charge transfer

detection. Using this technique, they obtained the total charge transfer cross-section, as a function of the vibrational state of H_2^+ (for states up to $v'=4$), at energies ranging from 8 to 200 eV (center of mass.) It was also found, that the low-lying rotational states of the H_2^+ ion had no discernible impact in the outcome of the reaction, at least when the ion was in its ground vibrational state and the collision energy was below 4 eV (c.m.) A strong dependency on the vibrational state was observed, with its maximum around 2 eV. It however decreases as the collision energy is reduced, contradicting the theoretical results trajectory surface hopping[90].

In a later experiment, with improved resolution, Liao and Ng[91] extended those results finding a good agreement with the semiclassical energy conserving trajectory calculations[92] at 16 eV, but with significant deviation at lower energies.

Other experiments include the use of pulsed synchrotron radiation and photoelectron-photoion coincidence to select the internal state of the H_2^+ ion, enabling the measurement of relative cross sections for states with $H_2^+(v'=0-10)$ at 16 eV.

The coupling among several vibrational states of the reactants and products was also observed for the CT channel in the energy range 8-400 eV, using the crossed beam technique[93].

CHAPTER 5 BASIS SETS AND ENERGETICS

Basis and H_4^+

As mentioned previously, only the two channels, CID and CT, are present at the energy range studied, in addition to the non-reactive one. A compilation of all the available theoretical and experimental data to date on the $H_2^+ + H_2$ reaction was provided by Phelps[94], and is shown in figure 5-1. A detail of the region analyzed here is presented in figure 5-2.

Before we present the results, we will discuss briefly the basis sets employed and our reasons to choose them. Due to the number of degrees of freedom involved, and the intensive computational nature of the END, our main concern is to find a basis that allows us to obtain a qualitative picture of the reaction, while minimizing the computer demand. Unlike the calculation of stationary states, in dynamics there is no common "feeling" of which basis will yield the desired results. That is especially true for END. In order to quantify how well each of the basis sets performs, we ran several calculations using an SCF wave function to minimize the energy of the projectile, the

target, and some relevant intermediates. It's known that H_4^+ is a stable molecule with a lifetime of about 10 μs , capable of supporting several vibrational levels[24]. It's also known that the SCF wave function can correctly describe that stability, yielding a ground state of C_{2v} symmetry[26].

Although it's generally accepted that H_4^+ cannot be formed by collisions between smaller molecules, but instead should arise only from breaking heavier fragments, an accurate depiction of the reaction energetics demands that at least the relative energies between the species involved are reasonably well reproduced.

We have chosen three different sets. Since our goal is to achieve a qualitative picture, we used the system energetics as a guide to initially gauge the performance of each. Here, we compare the results for the STO-3G basis, a double-zeta basis[95], and Dunning's pVDZ basis[96]. In a related calculation, the stability and geometry of H_4^+ was analyzed by Wright and Borkman[25]. Since they do not make clear what scaling factor they have used in their double-zeta case, if any, we have chosen to carry out the tests with the factor suggested by Dunning (1.44). To study the collisional process we use a factor equal to 1.54 for both the STO-3G and the DZ basis. The total energy at key points, involving intermediates, entrance and exit channel products was used to compare their effectiveness.

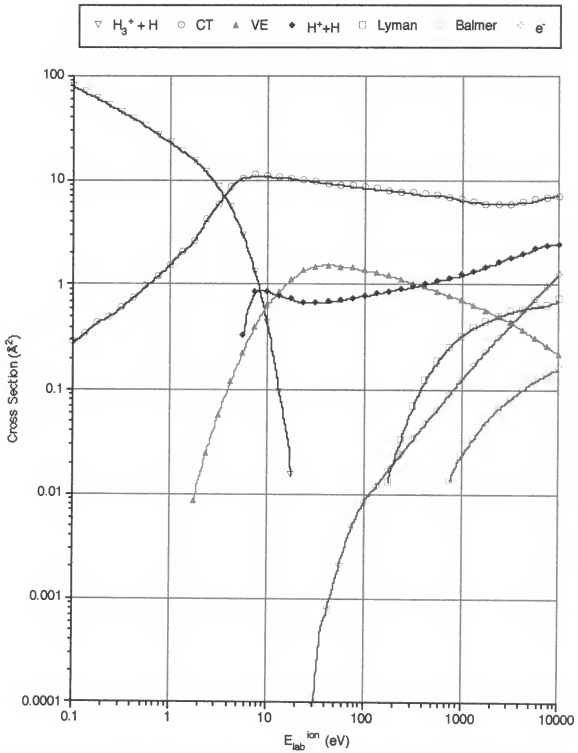


Figure 5-1: Available channels and cross-sections (\AA^2) for energies 0.1 to 10^5 eV (lab)

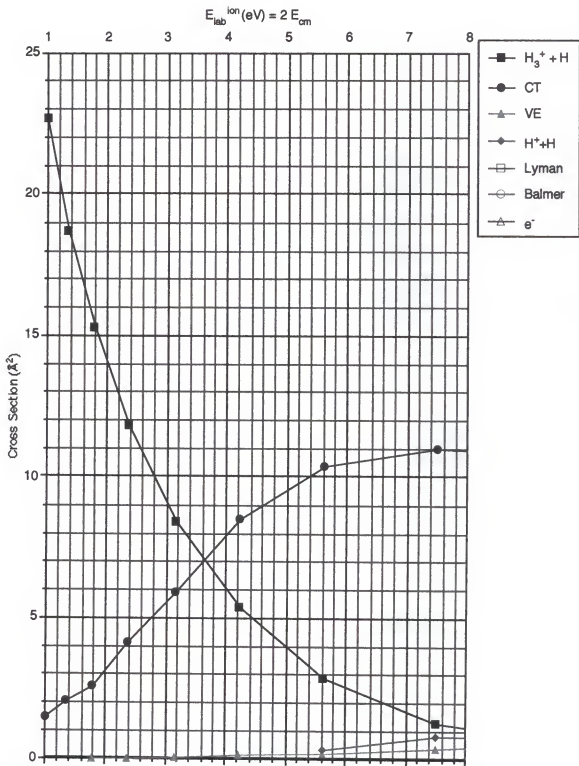


Figure 5-2: Cross-sections (\AA^2) for the range of energies studied, 1-8 eV (lab)

The three sets analyzed were the STO-3G, and Dunning's DZ, and pVDZ. Both the number of trajectories to sample the reaction space and the time necessary to simulate a single collision allowing for product separation are high. Since the END effort scales as N^4 , where N is the number of basis functions, the size of the basis is a major concern. In practical terms, we have limited this study to the DZ basis and the pVDZ is used only as a reference for selected initial conditions. The PVDZ basis is our benchmark set, being very successful in previous similar calculations on smaller systems. It also allows us to see how the introduction of polarization functions affect the results. A complete calculation of the reaction using this basis is not feasible due to the computer load imposed, requiring nearly 40 times the effort of a minimal basis. The DZ basis falls in between the previous two and gives an estimate of the importance of diffuse functions.

STO-3G Basis

This is a standard minimal basis, where a linear combination of three Gaussians has been fit to a single Slater-type function. The 1s orbital on each center is then represented by one of the resulting functions. The optimal fit for a Hydrogen atom, according this procedure yields the basis listed in table 5-1.

Table 5-1: Contraction coefficients (c) and exponents (α) for the STO-3G basis.

	c	α
1s orbital	0.44463	0.109818
	0.535328	0.405771
	0.154329	2.22766

The fitted exponents above were then modified to account for the tighter 1s orbitals in the reactants as compared to the atom. The scaling factor, 1.5376, was obtained from the Slater exponent, 1.24.

Dunning's DZ Basis[95]

The DZ basis has been used successfully by Wright and Borkman to study the stability of H_n^+ clusters, with n as high as 9. The resulting energies and geometries were comparable to a larger [5s,2p] basis.

Dunning's pVDZ Basis[96]

Table 5-2: Contraction coefficients (c) and exponents (α) for Dunning's pVDZ basis, with scaling factor 1.44.

	c	α
1s orbital	0.01969	18.7344
	0.13798	2.82528
	0.47815	0.64022
2s orbital	0.50124	0.17568
2p orbital	1.00000	0.72700

Energetics

In order to ascertain the performance of the above sets, we assume the reaction proceeds through a simple path going from the reactants, to the intermediate, to the products. The differences in energy between these points is compared in the three bases. The pVDZ results are considered as the reference values.

A geometry optimization, using a UHF wave function, was performed for each of the species involved. The calculations were not constrained to any particular point group, with the exception of the ones for the H_4^+ ion. In this case, the optimization was limited to the C_{2v} symmetry to accelerate convergence. This should not impose a major constraint, since the H_4^+ ground state is known to belong to the C_{2v} geometry. In all sets, H_3^+ converged to the D_{3h} point group, as expected. Table 5-3 contains the resulting total energies.

Table 5-3: Total energies, in atomic units, for the ground states

	STO-3G	DZ	pVDZ
H	-0.466582	-0.497637	-0.499278
H_2^+	-0.582697	-0.586387	-0.600286
H_2	-1.117506	-1.126658	-1.128746
H_3^+	-1.246860	-1.275824	-1.294005
H_4^+	-1.743480	-1.777434	-1.799292

Table 5-4: Bond lengths for the equilibrium geometries in the STO-3G basis, values in atomic units.

	R	R'	R''
H_2^+	2.00421	-	-
H_2	1.34592	-	-
$H_3^+(D_{3h})$	1.82718	1.82718	1.82718
$H_4^+(C_{2v})$	1.89523	2.24201	1.57174

Table 5-5: Bond lengths for the equilibrium geometries in the DZ basis, values in atomic units.

	R	R'	R''
H_2^+	1.98507	-	-
H_2	1.38142	-	-
$H_3^+(D_{3h})$	1.60570	1.60570	1.60570
$H_4^+(C_{2v})$	3.30625	1.64697	1.57097

Table 5-6: Bond lengths for the equilibrium geometries in the pVDZ basis, values in atomic units.

	R	R'	R''
H_2^+	1.98053	-	-
H_2	1.41343	-	-
$H_3^+(D_{3h})$	1.68039	1.68039	1.68039
$H_4^+(C_{2v})$	2.096235	1.74943	1.62159

In tables 5-4, 5-5, and 5-6 we list the equilibrium geometries for the above species. They essentially agree with values listed in the literature and confirm H_4^+ as a stable species. In table 5-8 we show the energies required to break H_4^+ into $H_2^+ + H_2$ (either CT or non-reactive), $H_3^+ + H$, and the total amount of energy released by CID. The energy barriers for the three sets is shown in figure 5-3 as the minimal energy path for the exit channel of a bond-breaking reaction ($H_2^+ + H_2 \rightarrow H_4^+ \rightarrow H_3^+ + H$) proceeding through a $C_{2v} H_4^+$ intermediate, and the reactants UHF surfaces in figure 5-4.

Table 5-7: Energetics in kcal/mol. Energy required to break H_4^+ into $H_2^+ + H_2$, $H_3^+ + H$, and total energy released by CID, respectively.

	$H_2^+ + H_2$	$H_3^+ + H$	ΔE
STO-3G	27.16	18.85	8.31
DZ	40.40	2.49	37.91
pVDZ	42.84	2.36	40.48

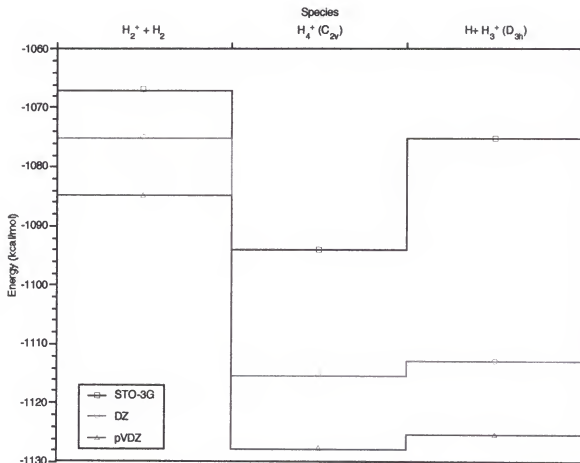


Figure 5-3: Energetics for the STO-3G, DZ, and pVDZ bases sets.

Some conclusions can be drawn from the above numbers. The stability of the H_4^+ species is a function of the basis size. As the basis become larger, going from the STO-3G set to the pVDZ, H_4^+ becomes more stable with respect to the entrance and the CT channels. The opposite happens for the CID channel. Increasing the basis makes it easier to have a collision resulting in dissociation.

UHF PES for the Reactants in Their Ground State

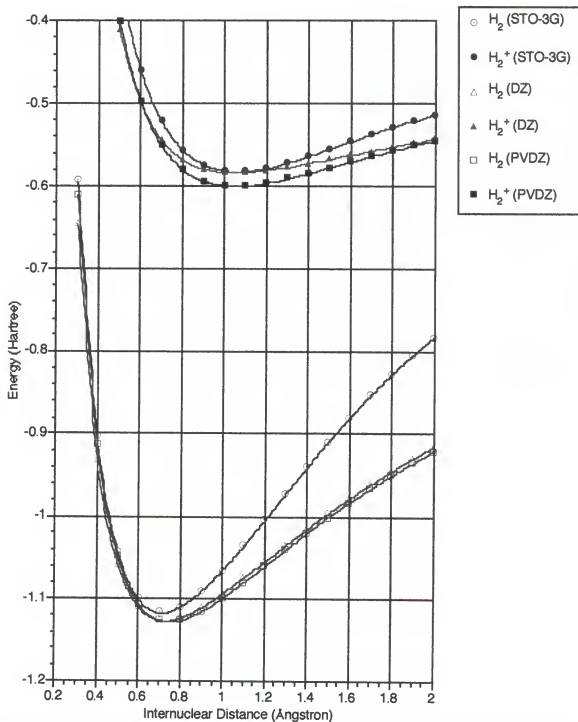


Figure 5-4: UHF ground-state surfaces for the STO-3G, DZ, and pVDZ bases

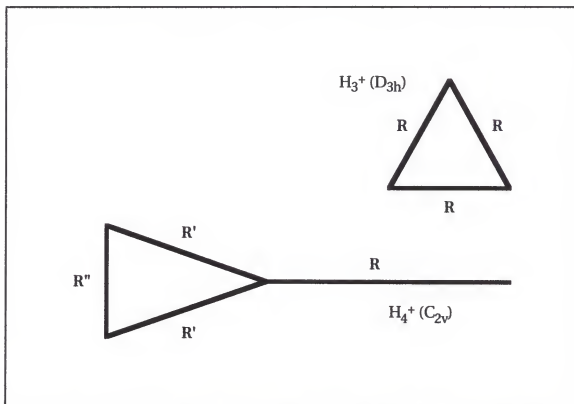


Figure 5-5: Bond lengths diagram for the H_3^+ and H_4^+ species in the D_{3h} and C_{2v} geometries, respectively

As a consequence, in the STO-3G basis, it is difficult to break the H_4^+ and, when it happens, the channels $H_2^+ + H_2$ and $H_3^+ + H$ will be more balanced than in larger basis. Between CT and CID, the later has a better chance. The DZ and pVDZ basis seem to perform about the same, at least in terms of energy differences.

It is interesting to note that the equilibrium geometry of H_4^+ in the STO-3G basis resembles the two reactants aligned perpendicularly. For the other two basis, the geometry is similar to an H_3^+ with an H atom aligned to one of the vertexes and orbiting far away from the H_3^+ core. That weak bond would make it more feasible to attain the CID channel.

It is clear that increasing the basis set reduces the H_4^+ stability. The percent relative difference between the DZ basis and the pVDZ one is just 5%. The DZ basis overshoots the exit barrier by about 5.5% of the pVDZ value, while the minimal basis requires over 7.5 times the energy when compared to the DZ number. Our results disagree with the findings of Wright and Borkman in that they report an increase in stability with the size of the basis. Their double-zeta result gives a bond-breaking energy of approximately 1.3 kcal/mol and a value of 3.2 kcal/mol for a [5s,2p] basis. That's too much of a discrepancy to be accounted for by differences in the scaling factor.

According to our numbers, the DZ should perform comparably to a pVDZ basis, at least in energetic terms. The minimal basis, while displaying the correct qualitative features of the larger sets, might lead to extremely stable H_4^+ intermediates, especially at lower values of collision energy.

CHAPTER 6 CROSS-SECTIONS

The full treatment of the $\text{H}_2^+ + \text{H}_2$ collision involves six internal nuclear degrees of freedom, corresponding to a choice of five parameters for the initial conditions. Consider the reactants in the lab frame, and take the z-axis as being the direction of the reaction. A single trajectory can be described by two tilt angles, a dihedral angle, and two impact parameters. The tilt angles refer to the inclination of each of the reactant bonds with respect to the z-axis. The dihedral angle is defined by planes formed by each of the reactant bonds and the z-axis. The two impact parameters are obtained from the distance between the center of the reactants and the z-axis. We show a diagram of the above in figure 6-1.

In order to obtain the total cross-sections, it is necessary to run several trajectories. Each trajectory is defined by a choice of initial conditions, which include the assignment of a value for each of the degrees of freedom. With five degrees of freedom, the number of possibilities increases quickly, making it important to devise a way to sample the reaction space without incurring in a prohibitively large calculation. For example, a relatively coarse grid with 6 points per degree of freedom, would

involve 7,776 trajectories. To decrease the mesh size to half of that would require 248,832 trajectories. Below, we explore a few possibilities to keep the calculation manageable.

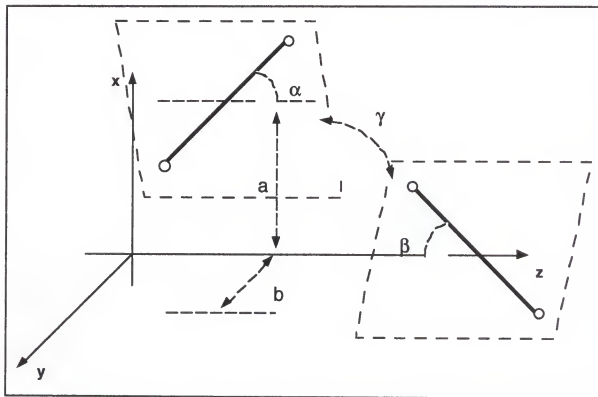


Figure 6-1: Degrees of freedom for the $\text{H}_2^+ + \text{H}_2$ reaction: α and β are the projectile and target tilt angles, respectively; γ is the dihedral angle; a and b are the impact parameters in the x and y directions, respectively.

The Collinear Approximation

The H_2 molecule, and to some extent the H_2^+ ion, possess an almost radial potential. This spherically symmetric potential suggests that the reactants could, in principle, be treated as atoms, which would reduce the problem to just one dimension. In fact, that idea has been used successfully in the past at energies of the order of 300 eV[97]. Although, it is more likely that the asymmetry of the potential plays a

rôle at low-energies, there is a possibility that this approximation could yield acceptable results concerning the total cross-sections. Since the calculation of the total cross-section involves averaging over all the degrees of freedom, any asymmetry could be averaged as well. To test that possibility, we performed calculations at very low energies, 0.519 eV, assuming both reactants as radially symmetric, and taking into account just one of the degrees of freedom.

The reduction in the number of trajectories, by considering just the impact parameter, is especially welcome at very low energies. To avoid unnecessary oscillations in the electronic populations, due to the overlap of the reactants' orbitals, the projectile and the target must be kept at a reasonably large separation. The higher the frequency of the oscillations, the harder the integrator has to work to keep track of the evolution, leading to extended computation time. This problem is somewhat alleviated for small basis sets, where the overlap is only significant at close range. For the $\text{H}_2^+ + \text{H}_2$ reaction, the total elimination of the interaction between the fragments is not possible, regardless of the amount of separation. The Coulomb interaction, due to the charged species, is always present, even at asymptotic distances. In this series of calculations, we use an initial separation of 20 a.u. between the centers of mass of the reactants.

Since we are assuming radial symmetry for both reactants, we must choose an initial spatial orientation for them which will be the same for every trajectory. It is important to notice that although we choose the initial orientation, the reactants are free to reorient as the reaction proceeds. This dynamically changing evolution is significantly less restrictive than some previous treatments of this system. A case in point is the full three-dimensional IOSA methodology[30]. Despite taking into account all the available degrees of freedom, the IOSA evolution makes no allowance for any re-orientation of the reaction participants[98]. For all practical purposes, the reactants are frozen in their initial orientations throughout the reaction. In our understanding, this is far more restrictive than a choice of fewer degrees of freedom, in particular for charge-transfer processes.

In our calculations we choose to put both projectile and target initially to lie parallel to the reaction coordinate. For that reason, we name this series the collinear approximation from now on.

As mentioned previously, the STO-3G basis yields exceptionally stable H_4^+ intermediates. This is especially critical at low-energies, where not enough translational energy from the projectile might be transferred into an appropriate vibrational mode of the intermediate to allow for a bond breaking. In our experience, this excessive stability renders the STO-3G basis unusable for energies below 1 eV.

The majority of the trajectories under these conditions yield the H_4^+ ion as a stable species even after 40,000 a.u. of time. For that reason, we choose instead to make use of a Dunning double-zeta set[95] in this series.

Collision Induced Dissociation

In table 6-1 we show the total cross-section for the CID channel, i.e., the one leading to $H_3^+ + H$ products. We have found this to be the prevalent channel for impact parameters above 0.6 a.u., and up to 5 a.u. An example of one such trajectories is given in figure 6-2. The first box shows the nuclear positions in the plane of the collision (xy plane), as the reaction proceeds. The bond lengths for both projectile and target are shown in the second box. From that, we can easily see the H_2 bond breaking, as its nuclei separate by up to 8 a.u. when the reaction reaches 8,000 a.u. of time. In the third box, we can see the changes in the Mulliken populations. The formation of the H_3^+ ion is clear above 5,000 a.u. of time. It is also apparent that the nucleus leaving as the H atom belonged originally to the target (H_2), and was the one facing the projectile. This is not always the case, and in figure 6-3 we show a trajectory, with impact parameter of 3 a.u., for which the leaving nucleus originally belonged to the projectile.

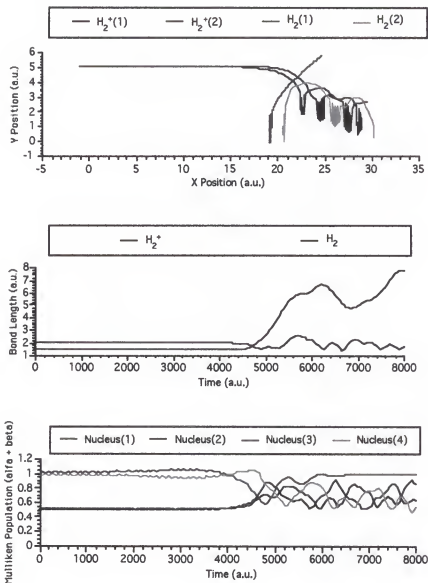


Figure 6-2: Collinear series, 0.519 eV, DZ basis, impact parameter 5 a. u.; top panel: nuclei trajectories on the xy plane; center panel: bond lengths vs. time; bottom panel: total Mulliken populations vs. time (all data in a. u.)

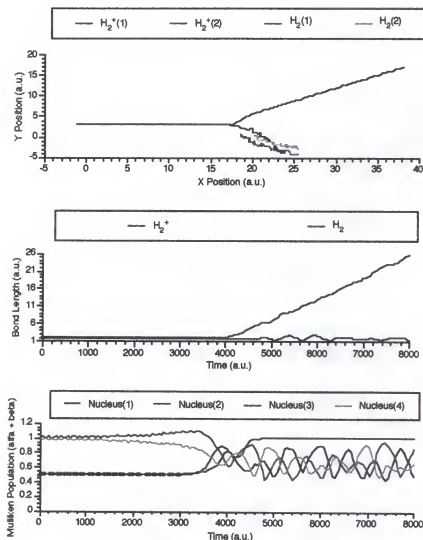


Figure 6-3: Collinear series, 0.519 eV, DZ basis, impact parameter 3 a. u.; top panel: nuclei trajectories on the xy plane; center panel: bond lengths vs. time; bottom panel: total Mulliken populations vs. time (all data in a. u.)

The total-cross section for the radial approximation is given by $\sigma = 2\pi \int P(b) b db$, where $P(b)$ is the probability, and b the impact parameter. Therefore, the contribution of a single trajectory increases with the square of its impact parameter.

We can project the final wave function to obtain the probabilities $P(\mathbf{b})$, as described earlier. We have found the main channel for each of trajectory to be totally predominant, with percentages higher than 99.9999%. In practice, $P(\mathbf{b})$ is either one or zero for any choice of impact parameter.

We also observed that there is no significant perturbation of the electronic populations for impact parameters above 6 a.u. and we take this value as the outer boundary for the reactive region.

The dominance of the CID in the outer portion of the reaction space accounts for its high cross-section, and seems to be in accordance with both the IOSA results (shown in table 6-1 as QM), and with the ones from semiclassical theory (SCL). All the three methods, END, QM[30], and SCL[45], seem to be in good agreement with each other and with the experimental results (Exp.)[99]. It is particularly notable that END shows a percentual relative deviation of just about 7.7%, with respect to experimental number.

Since the CID trajectories dominate the space close to the outer reactive shell, it is less likely that the choice of initial orientation for the reactants has any major impact on the final cross-sections.

Table 6-1: CID cross-sections, in \AA^2 , for 0.519 eV (CM), DZ basis

<i>CID</i>	<i>END</i>	<i>QM</i>	<i>SCL</i>	<i>Exp.</i>
σ	24.0	19	30 \pm 1	26 \pm 1

Charge Transfer

There are no available experimental results for the charge-transfer channel at this energy. In table 6-2 we list the IOSA, semiclassical[69], and END cross-sections.

This channel was found to be the dominant one for impact parameters from slightly above 0.3 a.u. to just less than 0.6 a.u. A representation of one such trajectory is given in figure 6-4. We can see, in the first panel, the products as two distinct vibrationally excited diatomic fragments. The second panel, shows the reactants exchanging bond lengths, indicating an electron transfer at around 4,000 a.u. of time. Notice the higher frequency and lower amplitude of the H_2 product. In the final panel, the Mulliken populations of the reactants are reversed, showing that the projectile(H_2^+) acquired one electron from the target.

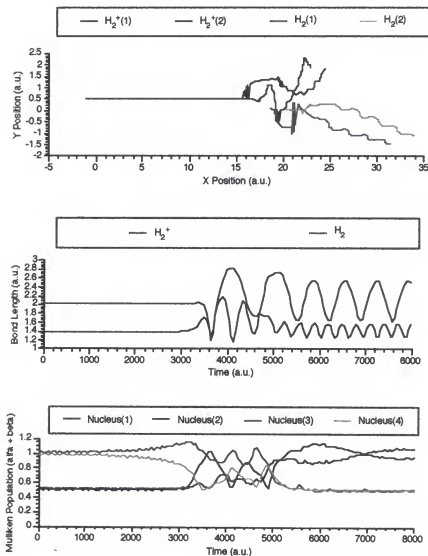


Figure 6-4: Collinear series, 0.519 eV, DZ basis, impact parameter 0.5 a. u.; top panel: nuclei trajectories on the xy plane; center panel: bond lengths vs. time; bottom panel: total Mulliken populations vs. time (all data in a. u.)

The CT process is extremely localized in terms of initial conditions and limited to small impact parameters. As a consequence, its contribution for the total cross-section is minimal. An extrapolation for the CT channel carried by Phelps[94], and shown in Figures 5-1 and 5-2, seems to

indicate that the correct value for this cross-section should be close to 1.5 \AA^2 . This is far less than what is obtained by SCL and, specially, the IOSA methods. Still, it is higher than the END result.

One possibility for this discrepancy might lie in the choice of initial conditions. By initially putting both reactants parallel to the reaction coordinate, we are effectively decreasing their level of interaction for small impact parameters. The combined half-bond lengths of the reactants would yield an extra 1.7 a.u. to the reaction shell, if aligned perpendicularly to the reaction coordinate. That would have a negligible effect on the CID channel, but could contain the major portion of the CT shell.

Studying the effects of the orientation on the cross-sections is beyond the scope of the collinear approximation and we leave it for a more detailed calculation, in the following sections.

As an illustration of the whole CT region, we present the projectile Mulliken population as a function of the impact parameter and evolution time, in figure 6-5. The projectile bond length is shown in a similar graph in figure 6-6. We can see in the lower right quadrant the increase in population (figure 6-5), and the decrease in bond length (figure 6-6).

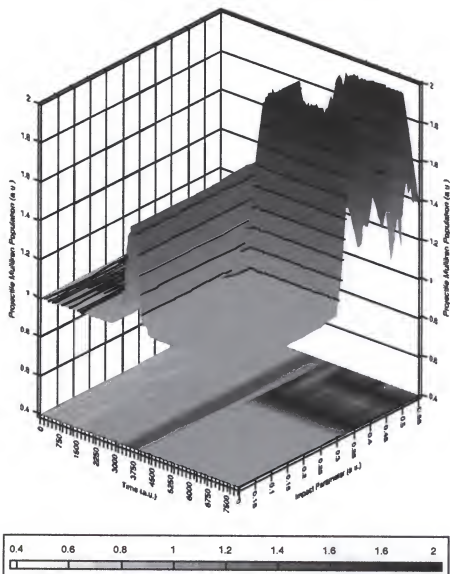


Figure 6-5: Collinear series, 0.519 eV, DZ basis; the projectile (H_2^+) total Mulliken population, as a function of time and impact parameter (all data in a. u.)

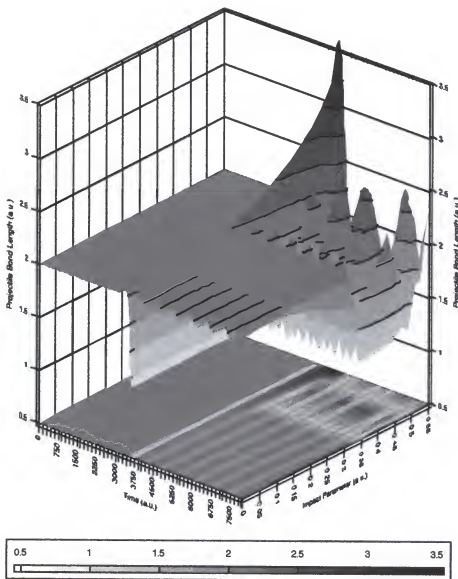


Figure 6-6: Collinear series, 0.519 eV, DZ basis; the projectile (H_2^+) bond length, as a function of time and impact parameter (all data in a. u.)

For the purpose of comparison, figure 6-7 depicts a non-reactive trajectory for an impact parameter of 0.3 a.u. This is the lower boundary of the CT channel and we can see its similarities with the collision shown in figure 6-4. The main differences occur in the region where the H_4^+ is formed,

around 4,000 a.u. of time. The non-reactive channel displays a temporary electron transfer, clearly visible in the Mulliken populations. As with the CT collision, the products leave in an excited vibrational state.

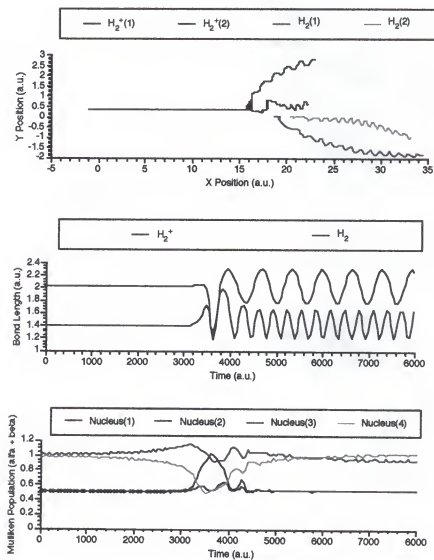


Figure 6-7: Collinear series, 0.519 eV, DZ basis, impact parameter 0.3 a. u.; top panel: nuclei trajectories on the xy plane; center panel: bond lengths vs. time; bottom panel: total Mulliken populations vs. time (all data in a. u.)

Table 6-2: CT cross-sections, in Å², for 0.519 eV (CM), DZ basis

CT	END	QM	SCL
σ	0.20	14	9±1

Full Reaction Space

At higher energies, the excessive stability of H_4^+ in the STO-3G basis is less of a problem. We learnt from practice that above 2 eV (CM) H_4^+ does not show up as a stable species, instead breaking up to yield a CT, a CID, or a NR product. On the other hand, from figure 5-2, we see that up to 4 eV (CM) it is feasible to carry on calculations without worrying about additional channels. At this collision energy, the evolutions are fast enough to allow us to be more comprehensive in the depth of treatment. With that in mind, we obtain the total cross-sections taking the full dimensionality of the reaction into account.

We employ the STO-3G basis, and a choice of initial conditions that span all the five degrees of freedom albeit in a limited way. These limitations include restricting the tilt angles to just three values, 30, 60, and 90 degrees. We also limit the dihedral angle to 30, 60, and 120 degrees. The impact parameters range from 0 to 6 a.u., in intervals of 1 or 2 a.u. Further, we assume the reaction to be symmetric

with respect to negative and positive impact parameters, decreasing the number of required trajectories to about one-fourth.

As it occurred with the 0.519 eV series, the probabilities for a given channel are sufficiently close to either 100% or zero for almost all the trajectories.

Collision Induced Dissociation

In figures 6-8 and 6-9, we show the reaction profiles for CID, in a variety of angles and impact parameters. Figure 6-8 groups the profiles for a dihedral angle of 30 degrees, and figure 6-9 for 60 degrees. It would seem likely by comparing those two groups of trajectories that the dihedral angle is playing little or no rôle in the outcome of the reaction. In figures 6-10 and 6-11, we present a more detailed view for the same channel but with a different choice of angles. The influence of the dihedral angle is now clear. These cases exemplify the difficulty of sampling the reaction space with a small number of trajectories. While figures 6-8 and 6-9 seem to point at some kind of symmetry that could be explored in order to reduce the number of required trajectories, it is not clear what the rule is. To determine it, a larger sampling of the space would be needed, which would defeat its purpose.

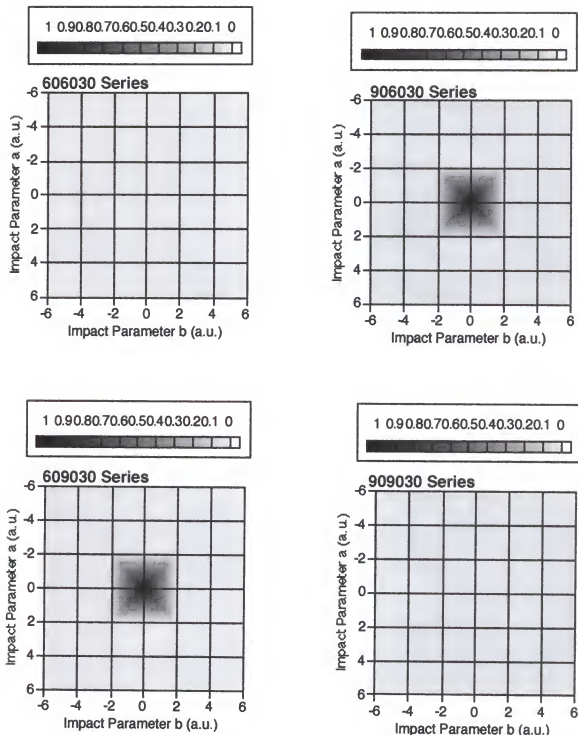


Figure 6-8: Bond breaking profiles for collision energy 4 eV and STO-3G basis; the shaded area marks the probability for the CID channel, as a function of both impact parameters (in a. u.); each series is labeled as $xyyz$, where xx is the projectile tilt angle, yy the target tilt angle, and zz the dihedral angle, all in degrees.

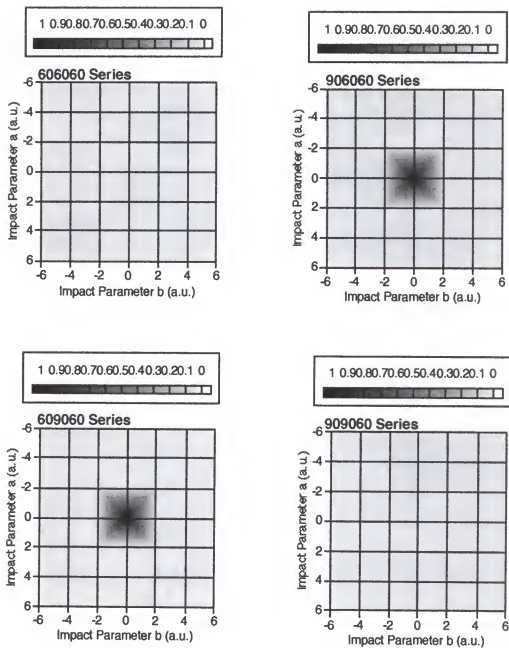


Figure 6-9: Bond breaking profiles for collision energy 4 eV and STO-3G basis; the shaded area marks the probability for the CID channel, as a function of both impact parameters (in a. u.); each series is labeled as xxyyzz, where xx is the projectile tilt angle, yy the target tilt angle, and zz the dihedral angle, all in degrees.

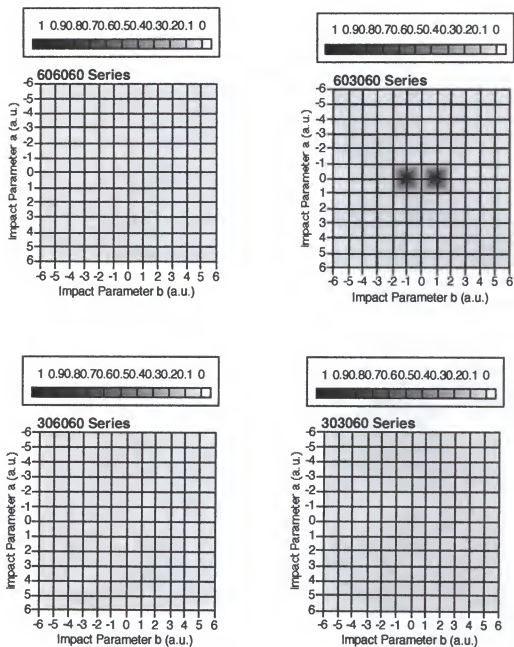


Figure 6-10: Bond breaking profiles for collision energy 4 eV and STO-3G basis; the shaded area marks the probability for the CID channel, as a function of both impact parameters (in a. u.); each series is labeled as $xyyzz$, where xx is the projectile tilt angle, yy the target tilt angle, and zz the dihedral angle, all in degrees.

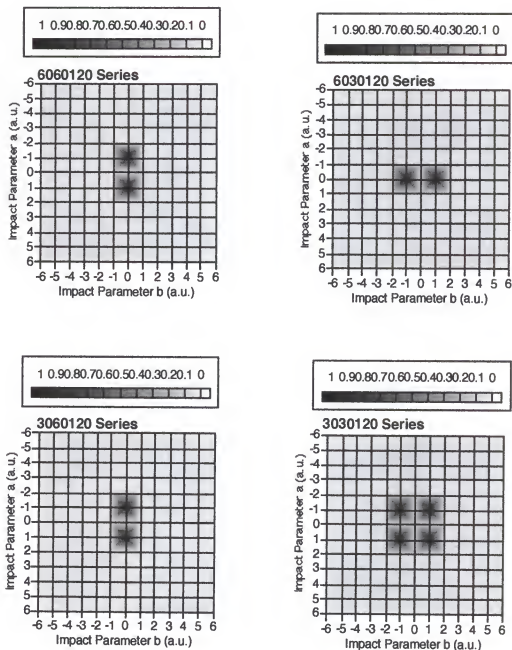


Figure 6-11: Bond breaking profiles for collision energy 4 eV and STO-3G basis; the shaded area marks the probability for the CID channel, as a function of both impact parameters (in a. u.); each series is labeled as xxyyzz, where xx is the projectile tilt angle, yy the target tilt angle, and zzz the dihedral angle, all in degrees.

It is also striking to note the difference in contrast to the reaction at low energies, where the CID channel was overwhelmingly prevalent. At 4 eV this is hardly the case, with only about 1% of the trajectories yielding $H_3^+ + H$. Another important distinction is the location of these CID trajectories, all of them lying close to the small impact parameters region. This is in accordance to the what is expected, and shown in figure 5-2. It is encouraging to see that even with a minimal basis set the correct behavior of the system prevails.

Table 6-3 compares the END total cross-section with both the trajectory-surface hopping(TSH)[42] method and the experimental value[58]. The discrepancy between the END result and the other two is within the precision of the grid of points used in the calculation. With so few reactive trajectories and a relatively coarse grid, it is reasonable to expect either missing a significant portion of the product, or "over-integrating" the outside boundary of the reaction shell.

Table 6-3: CID cross-sections, in \AA^2 , for 4 eV (CM), ST0-3G basis

<i>CID</i>	<i>END</i>	<i>TSH</i>	<i>Exp.</i>
σ	0.9	1.1	0.6

Charge Transfer

As we did for the CID channel, figures 6-12 and 6-13 display the reaction profiles for 60 and 90 degrees tilts, and 30 and 60 degrees dihedral. Once again, for this choice of angles, there is very little influence of the dihedral angle. With a finer grid and a different choice of angles, in figures 6-14 and 6-15, the reaction takes a different look. It shows a high asymmetry and a strong dependency on the choice of initial orientation.

The most important feature observed is, perhaps, the dominance of the CT channel at both large and small impact parameters. A marked difference in behavior when compared to energies below 1.5 eV. This holds true for any choice of initial conditions tested and we take it as a sign that the integration will give a good representation for this basis set, despite the strong asymmetry and sensitivity to the initial conditions.

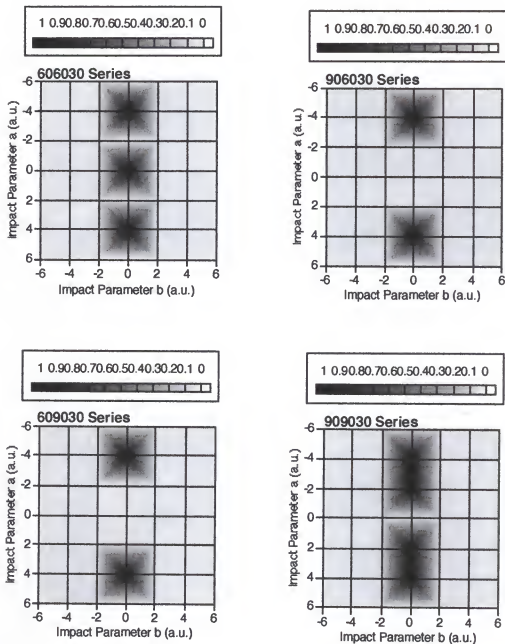


Figure 6-12: Charge transfer profiles for collision energy 4 eV and STO-3G basis; the shaded area marks the probability for the CT channel, as a function of both impact parameters (in a. u.); each series is labeled as xxyyzz, where xx is the projectile tilt angle, yy the target tilt angle, and zz the dihedral angle, all in degrees.

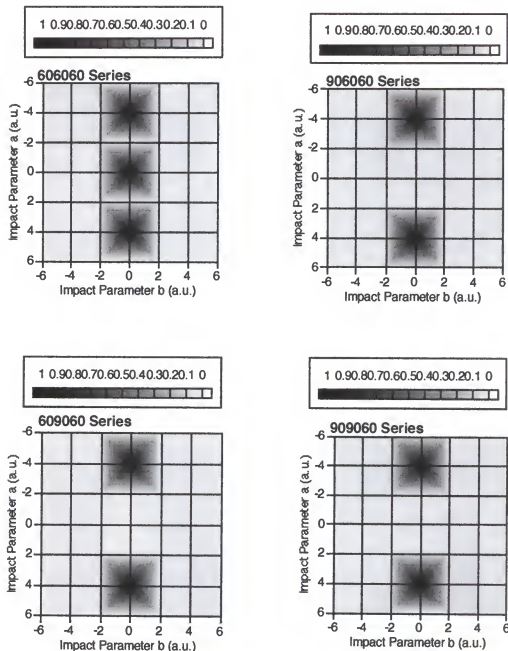


Figure 6-13: Charge transfer profiles for collision energy 4 eV and STO-3G basis; the shaded area marks the probability for the CT channel, as a function of both impact parameters (in a. u.); each series is labeled as $xxyyzz$, where xx is the projectile tilt angle, yy the target tilt angle, and zz the dihedral angle, all in degrees.

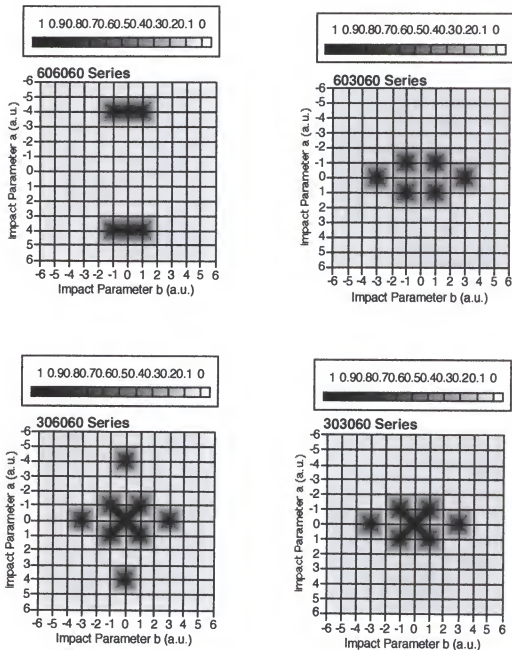


Figure 6-14: Charge transfer profiles for collision energy 4 eV and STO-3G basis; the shaded area marks the probability for the CT channel, as a function of both impact parameters (in a. u.); each series is labeled as xxxyzz, where xx is the projectile tilt angle, yy the target tilt angle, and zz the dihedral angle, all in degrees.

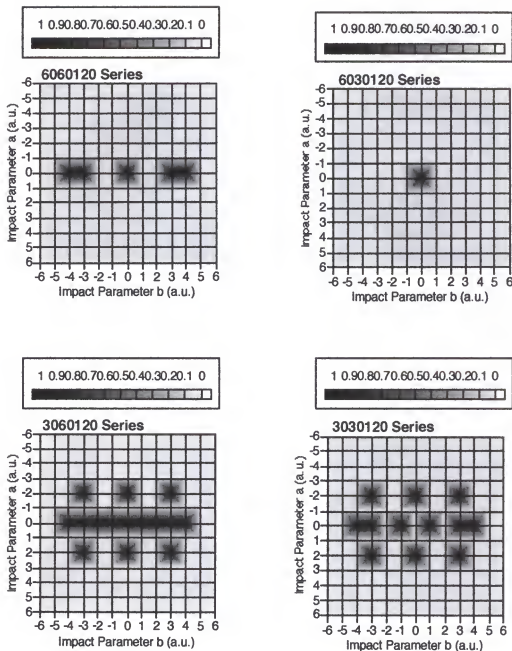


Figure 6-15: Charge transfer profiles for collision energy 4 eV and STO-3G basis; the shaded area marks the probability for the CT channel, as a function of both impact parameters (in a. u.); each series is labeled as xxyyzzz, where xx is the projectile tilt angle, yy the target tilt angle, and zzz the dihedral angle, all in degrees.

In table 6-4, we compare the total cross-sections as obtained from END, TSH, and experiment. Despite the small number of trajectories relative to the 40,000 in the TSH, END does remarkably well with a relative difference with respect to the experiment of just above 10%, compared to 103% for TSH.

Table 6-4: CT cross-sections, in \AA^2 , for 4 eV (CM), ST0-3G basis

CT	END	TSH	Exp.
σ	10.5	19.3	9.5

Comparison with Molecular Dynamics

Considering the integer probabilities we observed in the low-energy region, the question arises as to whether the electron-nuclei coupling is relevant for this system. And, if so, to what extent and in what form. To address this, we performed calculations using the molecular dynamics (MD) approach.

In particular, we have conducted the calculations using the dynamic reaction coordinate (DRC) methodology[100-102], as implemented in the software package GAMESS[103]. The DRC is a classical trajectory method, based on quantum chemical potential energy surfaces, which can be either *ab initio* or semi-empirical.

The initial conditions for a DRC trajectory are similar to the ones for END. One must provide the kinetic energy for

the reactants, as well as the direction of the initial velocity. We have chosen those to match the values of selected END trajectories. The spatial distribution of the reactants and their separation were made to agree as well.

There is a choice of wave-functions to describe the PES on which the DRC trajectory will evolve. We have selected the unrestricted Hartree-Fock (UHF) in the following examples.

Final Probabilities

Unlike END, the MD trajectories are constrained a single potential energy surface. As mentioned previously, almost all of the END evolutions for this system yielded 100% probability for the dominant channel. This is not an indication that these trajectories are limited to a single energy surface. However, it is more likely that we find the participation of higher lying surfaces for trajectories with split character (both channels present.)

One can measure the probability for each channel by projecting the final wave-function, representing the products, on the known wave-function for the desired fragment. In table 6-5, we shown the probabilities for a series of calculations, with initial conditions of 60 degrees for both tilt angles, and the dihedral angle, collision energy 4 eV, and a STO-3G basis. This series provided some of the largest deviations from unity probability, of all the series studied. It is clear that even for this set of calculations the deviation is minor. The trajectory with the

most pronounced split character is highlighted, and corresponds to the one with impact parameters 0 and 3 a. u., for the z and y directions, respectively. For this instance, the final probabilities are 8% for charge-transfer and 92% for the non-reactive channel.

Table 6-5: Probabilities for the final electronic configurations with initial conditions 606060 (4 eV, STO-3G). The shaded box displays the highest mixed character and a comparison between END and dynamics on a surface is provided for this case. (a, b are the impact parameters; CT: charge transfer; NR: non-reactive)

a (a.u.)	b (a.u.)	P _{CT}	P _{NR}	a (a.u.)	b (a.u.)	P _{CT}	P _{NR}
0	0	1.00	0.00	2	5	0.00	1.00
0	1	0.00	1.00	3	0	0.00	1.00
0	2	0.00	1.00	3	1	0.00	1.00
0	3	0.08	0.92	3	2	0.00	1.00
0	4	0.00	1.00	3	3	0.00	1.00
0	5	0.00	1.00	3	5	0.00	1.00
0	6	0.00	1.00	4	0	0.98	0.02
1	1	0.01	0.99	4	1	0.00	1.00
1	2	0.00	1.00	4	2	0.00	1.00
1	3	0.00	1.00	4	3	0.00	1.00
1	4	0.00	1.00	4	4	0.00	1.00
1	5	0.00	1.00	5	0	0.00	1.00
2	0	0.00	1.00	5	1	0.00	1.00
2	1	0.00	1.00	5	2	0.00	1.00
2	2	0.00	1.00	5	3	0.00	1.00
2	3	0.00	1.00	6	0	0.00	1.00
2	4	0.00	1.00				

In figure 6-16, we show the END evolution for the trajectory discussed. The first panel, represents the nuclei trails for the entire collision. The representation has been shifted to the center of mass to allow an easier comparison with the MD results. The projectile (H_2^+) is initially

situated at the origin, while the target sits at 15 a. u. As the reaction proceeds, both come into contact. They acquire some vibrational energy, which can be seen in the undulating motion of the nuclei (notice that H_2 mostly rotates around its center,) as the products leave the interaction region. The second panel shows the vibrational excitation more clearly, representing the bond lengths of the fragments. Most of the vibrational energy for this collision is transferred to the H_2^+ ion. The bond lengths also suggest there was no charge transfer, since they oscillate around their initial values for both fragments. This is confirmed in the third panel, where we show the total Mulliken population for each center, as a function of the evolution time.

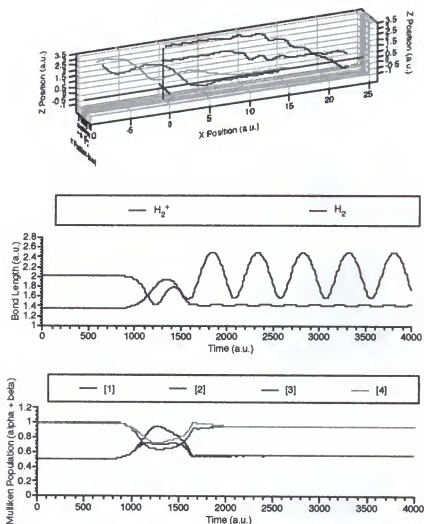


Figure 6-16: 606060 END series, 4 eV, STO-3G basis, impact parameters 3 and 0 a. u. (y and z axes, respectively); top panel: nuclei trajectories of the coordinates; center panel: bond lengths vs. time; bottom panel: total Mulliken populations vs. time (all data in a. u.)

Figure 6-17, displays the same trajectory above, this time obtained through the MD approach. A quick comparison shows the qualitative features of the END evolution are all present. The fragments follow roughly the same path, H_2^+ carries most of the final vibrational energy, and as before there is no charge transfer. There are however noticeable

changes in the amplitudes of vibration for both reactants. Such differences would not account for a change in the total cross sections, since the products would still be the same, but could certainly affect the distribution of final states.

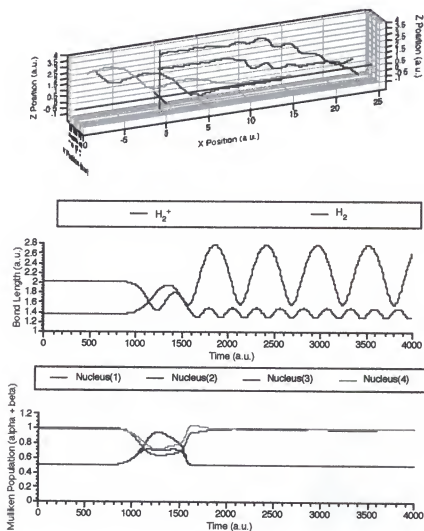


Figure 6-17: 606060 DRC series, 4 eV, STO-3G basis, impact parameters 3 and 0 a. u. (y and z axes, respectively); top panel: nuclei trajectories of the coordinates, respectively; center panel: bond lengths vs. time; bottom panel: total Mulliken populations vs. time (all data in a. u.)

pVDZ basis

A more sensitive way to gauge the difference between END and the MD, for this system, is perhaps a comparison involving a collision for which the prevalent channel results in charge transfer. As in the previous section, we choose a collision energy of 4 eV but, instead of the STO-3G basis, we use the more sensitive pVDZ set. For this example, we set the reactants initially lying parallel to the reaction coordinate, reducing the problem by one impact parameter, and making it simpler to interpret.

Figures 6-18 and 6-19 show an example of such trajectories for END and MD, respectively. Once again, we shifted the nuclei trajectories to the center of mass frame. It is apparent that both methods give comparable results. The main discrepancy being the vibrational states of the products, which show not only different amplitudes but also higher frequencies for END.

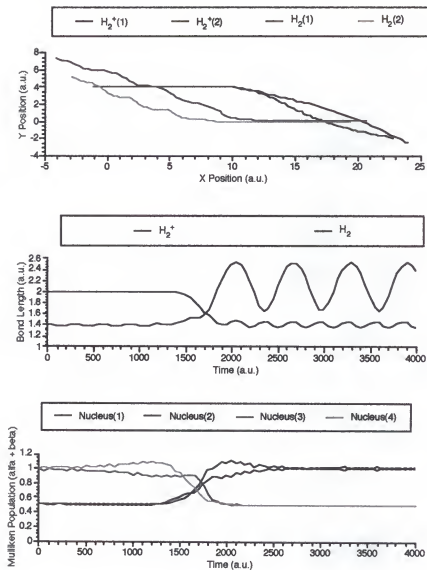


Figure 6-18: 000000 END series, 4 eV, pVDZ basis, impact parameters 0 and 4 a. u. (y and z axes, respectively); top panel: nuclei trajectories of the coordinates; center panel: bond lengths vs. time; bottom panel: total Mulliken populations vs. time (all data in a. u.)

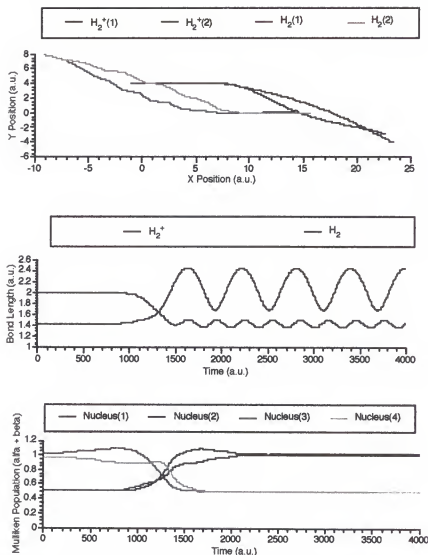


Figure 6-19: 000000 DRC series, 4 eV, pVDZ basis, impact parameters 0 and 4 a. u. (y and z axes, respectively); top panel: nuclei trajectories of the coordinates; center panel: bond lengths vs. time; bottom panel: total Mulliken populations vs. time (all data in a. u.)

CHAPTER 7 CONCLUSIONS

The $\text{H}_2^+ + \text{H}_2$ system has long been a favorite topic for both theoretical and empirical studies. In recent years, this interest has been revived, as the reaction not only displays both electron transfer and chemical exchange at energies low enough to be of chemical application, but also serves as a prototype for more complex ion-molecule interactions.

We have analyzed the reaction by using the electron nuclear dynamics (END) theory using a single determinantal wave function for the electrons and a classical description for the nuclei. The END results compare favorably with the existing "state of the art" approaches in both semi-classical and quantum methods.

We have found that the system energetics and dynamics can be qualitatively described by using small basis sets, even a minimal basis, provided the collision energy is large enough to allow for the dissociation of the H_4^+ intermediate. For energies below 2 eV, at least a DZ set is required. Also, the introduction of polarization functions, as in the case of the pVDZ set seems not to improve on the DZ results in terms of energetics.

Our calculations at 0.519 eV indicate that the reactants can be considered as radially symmetrical without too much

error. This approximation yields specially good results for the dominant channel (CID.) Since the chemical exchange region dominates the outer shell of the reaction space, it is unlikely the total cross-section for this channel could be significantly affected by the choice of initial orientations.

We obtain a charge transfer cross-section considerably lower than other theoretical approaches for the collinear approximation. One possible explanation for that is: since the CT region predominates only at small impact parameters, its area is comparable to the size of the bond lengths. In other words, the collinear approximation might be showing its shortcomings, by reducing the effective reaction shell. We should mention that both the semiclassical approach and the IOSA method grossly overestimate the cross-section reported by Phelps, which in itself seems to be extrapolated higher than what it should be.

The calculations exploring the full dimensionality of the system, at 4 eV, yield excellent results for both channels. They compare favorably to the semiclassical calculations, if the experimental result is taken as a reference.

It is somewhat surprising, how much the reaction profiles change with the choice of initial conditions for both channels. That seems to contradict the results based on the collinear approximation and, perhaps, point to an overall averaging over the spatial orientations.

We have found that the dynamics of the system is in almost its entirety deterministic concerning the products, for the range of energies studied, in the sense that only one channel is accessed for a given choice of initial conditions. This fact, and the range of low-energies we considered, appears to indicate the reaction proceeds mainly on a single PES. A comparison with the molecular dynamics approach for some of the most critical cases supports that and does not seem to be dependent on the size of the basis set, at least as far as the total cross-sections are involved. At higher energies, as well as for properties dependent on the vibrational state of the products, this might not be the case.

LIST OF REFERENCES

1. Herzberg, G., Nature **163**, 170 (1949).
2. Joseph, R.D., Wright, G.S., & Wade, R., Nature **311**, 132 (1984).
3. Kolos, W. & Wolniewicz, L., The Journal of Chemical Physics **49**(1), 404-410 (1968).
4. Dehmer, P.M. & Chupka, W.A., Journal of Physical Chemistry **99**(6), 1686-1699 (1995).
5. Thomson, J.J., Philos. Mag. **24**, 209 (1912).
6. Dempster, A.J., Philos. Mag. **31**, 438 (1916).
7. Acuña, M.H., Neubauer, F.M., & Ness, N.F., J. Geophys. Res. **86**, 8513 (1981).
8. Bohr, N., Medd. K. Vet.-Akad: S. Nobelinstitut **5**, 1 (1919).
9. Hirschfelder, J.O., Journal of Chemical Physics **6**(795)(1938).
10. Salmon, L. & Poshusta, R.D., J. Chem. Phys. **59**, 3497 (1973).
11. Gaillard, M.J., Gemmell, D.S., Goldring, G., Levine, I., Pietsch, W.J., Poizat, J.C., Ratkowski, A.J., Remillieux, J., Vager, Z., & Zabransky, B.J., Phys. Rev. A **17**, 1797 (1978).
12. Frye, D., Preiskorn, A., Lie, G.C., & Clementi, E., J. Chem. Phys. **92**, 4948 (1990).

13. Geballe, T.R. & Oka, T., *Astrophys. J.* **342**, 855 (1989).
14. Dalgarno, A., *TERRESTRIAL AND EXTRATERRESTRIAL H_3^+* , in
ADVANCES IN ATOMIC, MOLECULAR, AND OPTICAL PHYSICS.
1994, Academic Press, Inc.: p. 57-68.
15. Saporoschenko, M., *Phys. Rev. A* **139**, 349 (1965).
16. Lie, G.C. & Frye, D., *J. Chem. Phys.* **96**(9), 6784-6790
(1992).
17. Frye, D., Preiskorn, A., Lie, G.C., & Clementi, E.
Modern Techniques in Computational Chemistry. in *ESCOM.*
1990. Leiden: ESCOM.
18. Oka, T., *Phys. Rev. Lett.* **45**, 531 (1980).
19. Carney, G.D. & Porter, R.N., *J. Chem. Phys.* **64**, 4251
(1974).
20. Carney, G.D. & Porter, R.N., *J. Chem. Phys.* **65**, 3547
(1976).
21. Meyer, E., Botschwina, P., & Burton, P., *J. Chem. Phys.*
84, 891 (1986).
22. Miller, S. & Tennyson, J., *J. Mol. Spectrosc.* **128**, 530
(1988).
23. Miller, S. & Tennyson, J., *J. Mol. Spectrosc.* **136**, 223
(1989).
24. Kirchner, N.J., Gilbert, J.R., & Bowers, M.T., *Chemical
Physics Letters* **106**(1,2), 7-12 (1984).
25. Borkman, R.F. & Cobb, M., *J. Chem. Phys.* **74**, 2920
(1981).
26. Wright, L.R. & Borkman, R.F., *The Journal of Chemical
Physics* **77**(4), 1938-1941 (1982).

27. Poshusta, R.D. & Zetik, D.F., The Journal of Chemical Physics **58**(1), 118-125 (1973).
28. Borkman, R.F. & Cobb, M., The Journal of Chemical Physics **74**(5), 2920-2926 (1981).
29. Deumens, E., Diz, A., Taylor, H., & Öhrn, Y., The Journal of Chemical Physics **96**(9), 6820-6833 (1992).
30. Baer, M. & Ng, C.Y., The Journal of Chemical Physics **93**(11), 7787-7799 (1990).
31. Tully, J.C., The Journal of Chemical Physics **59**(9), 5122-5134 (1973).
32. Karplus, M., Porter, R.N., & Sharma, R.D., The Journal of Chemical Physics **59**, 4393 (1965).
33. McLaughlin, D.R. & Thompson, D.L., Journal of Chemical Physics **59**, 4393 (1973).
34. Sathyamurthy, N., Kellerhals, G.E., & Raff, L.M., The Journal of Chemical Physics **64**(5), 2259-2261 (1976).
35. Sathyamurthy, N., Rangarajan, R., & Raff, L.M., Journal of Chemical Physics **64**, 4606 (1976).
36. Gray, S.K. & Wright, J.S., Journal of Chemical Physics **66**, 2867 (1977).
37. Miller, W.H. & George, T.F., The Journal of Chemical Physics **56**(11), 5637-5652 (1972).
38. Tully, J.C. & Preston, R.K., Journal of Chemical Physics **55**, 562 (1971).
39. Stine, J.R. & Muckerman, J.T., Chemical Physics Letters **44**(1), 46-49 (1976).

40. Preston, R.K., Sloane, C., & Miller, W.H., *Journal of Chemical Physics* **60**, 4961 (1974).
41. Lin, Y.-W., George, T.F., & Morokuma, K., *Chemical Physics Letters* , 49 (1975).
42. Eaker, C.W. & Schatz, G.C., *The Journal of Chemical Physics* **89**(11), 6713-6718 (1988).
43. Schatz, G.C., Badenhop, J.K., & Eaker, C.W., *International Journal of Quantum Chemistry XXXI*, 57-63 (1987).
44. Eaker, C.W. & Schatz, G.C., *The Journal of Physical Chemistry* **89**, 2612 (1985).
45. Eaker, C.W. & Schatz, G.C., *Chemical Physics Letters* **127**(4), 343-346 (1986).
46. Neuhauser, D. & Baer, M., *Journal of Chemical Physics* **93**, 2862 (1989).
47. Neuhauser, D. & Baer, M., *Journal of Chemical Physics* **94**, 185 (1990).
48. Kosloff, R., *Journal of Chemical Physics* **92**, 2087 (1988).
49. Kosloff, R. & Kosloff, D., *Journal of Chemical Physics* **94**, 185 (1990).
50. Kramer, P. & Saraceno, M., *Geometry of the Time-Dependent Variational Principle in Quantum Mechanics*. 1981, New York: Springer.
51. Klauder, J.R. & Skagerstam, B.-S., *COHERENT STATES - APPLICATIONS IN PHYSICS AND MATHEMATICAL PHYSICS*. 1st

- ed. 1985, Singapore: World Scientific Publishing Co. Pte. Ltd. 911.
52. Perelomov, A.M., *Generalized Coherent States and Their Applications*. 1st ed. Texts and Monographs in Physics, eds. W. Beiglböck, et al. 1986, Berlin, Germany: Springer-Verlag. 320.
 53. Deumens, E., Öhrn, Y., & Weiner, B., *Journal of Mathematical Physics* **32**, 1166 (1991).
 54. Delos, J.B., *Review of Modern Physics* **58**, 287 (1981).
 55. Thouless, D.J., *Nuclear Physics* **21**, 225 (1960).
 56. Herbst, E. & Klemperer, W., *Astrophys. J.* **183**, 117 (1973).
 57. Prasad, S.S. & Tan, A., *Geophys. Res. Lett.* **1**, 337 (1979).
 58. Guyon, P.M., Baer, T., Cole, S.K., & Govers, T.R., *Chemical Physics* **119**, 145-158 (1988).
 59. Krenos, J.R., LLehman, K.K., Tully, J.C., Hierl, P.M., & Smith, G.P., *Chem. Phys.* **16**, 109 (1976).
 60. Hierl, P.M. & Herman, Z., *Chem. Phys.* **50**, 249 (1980).
 61. Vance, D.W. & Bailey, T.L., *The Journal of Chemical Physics* **44**(2), 486-493 (1966).
 62. Futrell, J.H. & Abramson, F.P., *Adv. Chem. Ser.* **58**, 123 (1966).
 63. Douglass, C.H., McClure, D.J., & Gentry, W.R., *The Journal of Chemical Physics* **67**(11), 4931-4940 (1977).
 64. Lees, A.B. & Rol, P.K., *The Journal of Chemical Physics* **61**(11), 4444-4449 (1974).

65. Chupka, W.A. & Russell, M.E., The Journal of Chemical Physics **49**(12), 5426-5437 (1968).
66. Huntress, W.T., Elleman, D.D., & Bowers, M.T., J. Chem. Phys. **55**, 5413 (1971).
67. Doverspike, L.D. & Champion, R.L., J. Chem. Phys. **46**, 4718 (1967).
68. Anderson, S.L., Hirooka, T., Tiedemann, P.W., Mahan, B.H., & Lee, Y.T., J. Chem. Phys. **73**, 4479 (1980).
69. Muckerman, J.T., Theoretical Chemistry **6**, 1 (1981).
70. Koyono, I. & Tanaka, K., J. Chem. Phys. **72**, 4858 (1980).
71. Stine, J.R. & Muckerman, J.T., The Journal of Chemical Physics **68**(1), 185-194 (1978).
72. Cobb, M., Moran, T.F., Borkman, R.F., & Childs, R., Chem. Phys. Lett. **57**, 326 (1978).
73. Anderson, S.L., Houle, F.A., Gerlich, D., & Lee, Y.T., The Journal of Chemical Physics **75**(5), 2153-2162 (1981).
74. Pollard, J.E., Johnson, L.K., Lichtin, D.A., & Cohen, R.B., The Journal of Chemical Physics **95**(7), 4877 (1991).
75. Polak, R., Chem. Phys. **16**, 353 (1976).
76. Latimer, C.J., Browning, R., & Gilbody, H.B., J. Phys. B **2**, 1055 (1969).
77. Hayden, H.C. & Amme, R.C., Phys. Rev. **172**, 104 (1968).
78. Cramer, W.H., J. Chem. Phys. **35**, 836 (1961).
79. Rothwell, H.L., Zyl, B.V., & Ame, R.C., J. Chem. Phys. **61**, 3851 (1974).

80. Wolf, F., Ann. Phys. **29**, 33 (1937).
81. Simons, J.H., Fontana, C.M., E. E. Muschlitz, J., & Jackson, S.R., J. Chem. Phys. **11**, 312 (1943).
82. Moran, T.F. & Roberts, J.R., J. Chem. Phys. **49**, 3411 (1968).
83. Stedeford, J.B.H. & Hasted, J.B., Proc. R. Soc. London Ser. A **227**, 466 (1955).
84. Cramer, W.H. & Marcus, A.B., J. Chem. Phys. **32**, 186 (1960).
85. Hollricher, O., Z. Phys. **187**, 41 (1965).
86. Koopman, D.W., Phys. Rev. **154**, 79 (1967).
87. Liao, C.-L., Liao, C.-X., & Ng, C.Y., The Journal of Chemical Physics **81**(2), 5672-5691 (1984).
88. Chupka, W.A., , in *Ion-Molecule Reactions*, J.L. Franklin, Editor. 1972, Plenum: New York. p. 33.
89. Campbell, F.M., Browning, R., & Latimer, C.J., J. Phys. B **14**, 3493 (1981).
90. Muckerman, J.T., , in *Theoretica Chemistry*, D. Henderson, Editor. 1981, Academic: New York. p. 1.
91. Liao, C.L. & Ng, C.Y., J. Chem. Phys. **84**(1), 197-200 (1986).
92. Lee, C.-Y. & DePristo, A.E., The Journal of Chemical Physics **80**(3), 1116-1125 (1984).
93. Lee, C.-Y., Depristo, A.E., Liao, C.-L., & Ng, C.Y., Chemical Physics Letters **116**(6), 534 (1985).
94. Phelps, A.V., Journal of Physical Chemistry Reference Data **19**(3), 653-674 (1990).

95. Dunning, T.H., Jr., The Journal of Chemical Physics 53(7), 2823-2833 (1970).
96. Dunning, T.H., Jr., The Journal of Chemical Physics 90(2), 1007-1023 (1989).
97. Giese, C.F. & II, W.B.M., The Journal of Chemical Physics 39(3), 739-748 (1963).
98. Baer, M. & Nakamura, H., The Journal of Physical Chemistry 91, 5503-5509 (1987).
99. Shao, J.D. & Ng, C.Y., The Journal of Chemical Physics 84(8), 4317-4325 (1986).
100. Stewart, J.J.P., Davis, L.P., & Burggraf, L.W., J. Comput. Chem. 8, 1117-1123 (1987).
101. Maluendes, S.A. & Dupuis, M., J. Chem. Phys. 93, 5902-5911 (1990).
102. Taketsugu, T. & Gordon, M.S., J. Phys. Chem. 99, 8462-8471 (1995).
103. Schmidt, M.W., Baldridge, K.K., Boatz, J.A., Elbert, S.T., Gordon, M.S., Jensen, J.J., Koseki, S., Matsunaga, N., Nguyen, K.A., Su, S., Windus, T.L., Dupuis, M., & Montgomery, J.A., J. Comput. Chem. 14, 1347-1363 (1993).

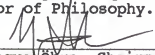
BIOGRAPHICAL SKETCH

Juan Oreiro was born in Rio de Janeiro, Brazil. He enrolled in Chemical Engineering at Federal University of Rio de Janeiro (EQ-UFRJ.) As an undergraduate he received scholarships for scientific research in the fields of organic synthesis and analysis, natural products, and inorganic synthesis.

After graduation he enrolled in a Master's degree in Chemistry, at the Institute of Chemistry-UFRJ. During that period he received a scholarship from the Brazilian government and started doing research in Quantum Chemistry.

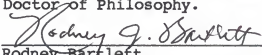
When visiting Gainesville, during the 1988 Winter Institute on Quantum Chemistry he met Professor Öhrn. Later, he came to the University of Florida and joined the Öhrn-Deumens group.

I certify that I have read this study and that in my opinion it conforms to acceptable standards of scholarly presentation and is fully adequate, in scope and quality, as a dissertation for the degree of Doctor of Philosophy.



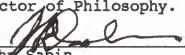
N. Yngve Ohrn, Chairman
Professor of Chemistry

I certify that I have read this study and that in my opinion it conforms to acceptable standards of scholarly presentation and is fully adequate, in scope and quality, as a dissertation for the degree of Doctor of Philosophy.



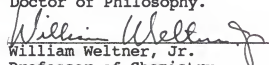
Rodney Bartlett
Graduate Research Professor
of Chemistry

I certify that I have read this study and that in my opinion it conforms to acceptable standards of scholarly presentation and is fully adequate, in scope and quality, as a dissertation for the degree of Doctor of Philosophy.



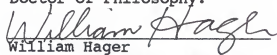
John Sabin
Professor of Physics

I certify that I have read this study and that in my opinion it conforms to acceptable standards of scholarly presentation and is fully adequate, in scope and quality, as a dissertation for the degree of Doctor of Philosophy.



William Weltner, Jr.
Professor of Chemistry

I certify that I have read this study and that in my opinion it conforms to acceptable standards of scholarly presentation and is fully adequate, in scope and quality, as a dissertation for the degree of Doctor of Philosophy.



William Hager
Professor of Mathematics

This dissertation was submitted to the Graduate Faculty of the Department of Chemistry in the College of Liberal Arts and Sciences and to the Graduate School and was accepted as partial fulfillment of the requirements for the degree of Doctor of Philosophy.

December, 1997

Dean, Graduate School